JOURNAL OF QUATERNARY SCIENCE (2022) 1–19 ISSN 0267-8179. DOI: 10.1002/jqs.3407

JQS Journal of Quaternary Science QRA Quaternary Research Association

Late Pleistocene glaciation history of the southern Black Forest, Germany: ^{10}Be cosmic-ray exposure dating and equilibrium line altitude reconstructions in Sankt Wilhelmer Tal

FELIX MARTIN HOFMANN,[1]* FRANK PREUSSER,[1] IRENE SCHIMMELPFENNIG,[2] LAËTITIA LÉANNI[2] and ASTER TEAM (GEORGES AUMAÎTRE, KARIM KEDDADOUCHE & FAWZI ZAIDI)[2]

[1]Institute of Earth and Environmental Sciences, University of Freiburg, Freiburg, Germany
[2]Aix-Marseille Université, CNRS, IRD, INRAE, Aix-en-Provence, France

Received 1 September 2021; Revised 17 December 2021; Accepted 23 December 2021

ABSTRACT: During the Late Pleistocene, an ice cap temporarily rested on the highest summit of the Black Forest, Feldberg, and on the surrounding region. Moraines inside the last glaciation maximum ice extent document subsequent glacial standstills and/or re-advances, but the chronology of the deglaciation remains largely unknown. In Sankt Wilhelmer Tal, moraines were mapped, and suitable moraine boulders were sampled for ^{10}Be cosmic ray exposure (CRE) dating. Equilibrium line altitudes (ELAs) during moraine formation were reconstructed to evaluate whether these can be used for local stratigraphical correlations. Geomorphological mapping revealed numerous ice-marginal positions in the main valley and in two tributary valleys. CRE ages and ELAs indicate two discrete phases of glacial standstills and/or re-advances by 17–16 ka at the latest and no later than 14 ka, respectively. Differing ELAs across the study area preclude the use of ELAs for local stratigraphical correlations. Recalculated ^{10}Be CRE ages from other localities in Central Europe indicate similar periods of moraine formation, thus raising the question of a common climatic forcing. Additional sets of CRE ages are needed to answer this question. In addition, future studies should concentrate on determining the age of the last glaciation maximum in the Black Forest.

KEYWORDS: ^{10}Be cosmic-ray exposure dating; Black Forest; equilibrium line altitude; glaciation; moraine

Introduction

The geomorphological record of ice sheets, ice caps and glaciers is commonly employed for the reconstruction of past climatic changes (e.g. Stokes *et al.*, 2015; Rea *et al.*, 2020). If factors other than climate, such as topography (Barr and Lovell, 2014), do not significantly influence their mass balance, variations in ice extent document changes in precipitation and/or temperature (e.g. Kerschner and Ivy-Ochs, 2008). Information on the past extent of smaller ice bodies is particularly valuable, as they dynamically react to both climatic trends on long timescales and short-term climatic shifts (Mackintosh *et al.*, 2017).

Research on the landform record of small-scale Quaternary glaciations in low mountainous areas of Central Europe (*Mittelgebirge*) has a long tradition. Traces of the glaciations of the Black Forest and Vosges were first recognized and described in the first half of the 19th century (Haase, 1966; Mercier and Jeser, 2004) when the theory of widespread past glaciations was developed in the Alps. Since then, glacial landforms in low mountainous regions in Central Europe have been systematically investigated and mapped (Steinmann, 1902; Ergenzinger, 1967; Duphorn, 1968; Andreoli *et al.*, 2006; Krause and Margold, 2019). The study of sediments in lakes and mires inside of moraines has provided insights into the chronology of the glaciations (Woillard, 1978; Lang *et al.*, 1984; Vočadlová *et al.*, 2015). The emergence of cosmic-ray exposure (CRE) dating in the 1990s greatly facilitated determination of the age of ice-marginal positions. The first CRE ages from a low mountainous area in Central Europe were acquired in the Vosges (Mercier *et al.*, 1999) and the Giant Mountains (Mercier *et al.*, 2000). Further sets of CRE ages of moraines were later obtained for the Bavarian Forest (Reuther, 2007), the Bohemian Forest (Mentlík *et al.*, 2013) and for the Giant Mountains (Engel *et al.*, 2011;).

Well-preserved moraines are found at various localities in the southern Black Forest (Liehl, 1982; Metz and Saurer, 2012; Hemmerle *et al.*, 2016), but they have hitherto not been directly dated. The outermost of these landforms indicate the presence of a 1000-km^2 ice cap during the Late Pleistocene. It covered the highest summit of the Black Forest, Feldberg [1493 m above sea level (a.s.l.)], and the surrounding region (Liehl, 1982; Metz and Saurer, 2012; Hemmerle *et al.*, 2016). The outlet glaciers of this ice cap were up to 25 km long (Hemmerle *et al.*, 2016) and one of them had a maximum thickness of 440 m (Sawatzki, 1992). Groups of morphostratigraphically younger moraines have been preserved inside the supposed maximum ice extent of the last glaciation. A recent geomorphological study revealed numerous ice-marginal positions in the area NW of Feldberg (Hofmann *et al.*, 2020), but the chronology of their formation remains largely unknown. The only conclusions on the deglaciation chronology were drawn by analogy with data from sediment cores from lakes and mires inside of moraines (summarized in Lang, 2005). As the estimation of the age of the lithostratigraphic units in the cores relies only on the apparent, but not properly documented presence of the Laacher See Tephra and not on radiocarbon ages, the suggested chronological correlations should be considered with greatest caution.

*Correspondence: Felix Martin Hofmann, as above.
Email: felix.martin.hofmann@geologie.uni-freiburg.de

The moraines in the southern Black Forest represent prime candidates for palaeoclimatological reconstructions, as the high number of ice-marginal positions suggests highly dynamic glaciers. Dating the former glacier extents could thus provide information on both long-term climatic trends and climatic oscillations on short timescales. In addition, the use of glaciers as palaeoclimatological archives would allow us to compensate for the scarcity of biological proxies in mountainous regions of Central Europe. Sedimentary records from these areas documenting palaeoenvironmental changes before the rapid warming at around 14.6 ka are scarce (Maier *et al.*, 2021), with only a few exceptions (Becker *et al.*, 2006; Duprat-Oualid *et al.*, 2017).

Establishing a robust chronology of glacier fluctuations in the Black Forest represents a prerequisite for glacier-based palaeoclimatological reconstructions. As previously mentioned (Hofmann *et al.*, 2020), suitable boulders for CRE dating exist on most of the moraines in Sankt Wilhelmer Tal, a valley NW of Feldberg. Since quartz-rich lithologies dominate the valley (Hann *et al.*, 2011), this area was deemed particularly suitable to obtain the first ^{10}Be CRE ages for moraines of the Black Forest. Equilibrium line altitudes (ELAs) during moraine formation were reconstructed to assess whether palaeo-ELAs can be employed for local stratigraphical reconstructions. To evaluate whether the reconstructed chronology is consistent with existing chronologies from mountain regions in Central Europe, previously published ^{10}Be CRE ages from these areas were recalculated according to recent ^{10}Be production parameters.

Study area and previous work

Study area

The study area consists of Sankt Wilhelmer Tal *sensu strictu* as well as two tributary valleys, Wittenbach and Katzensteig (Fig. 1). The upper part of the main valley is commonly referred to as Napf. The study area is delimited to the south by the Stübenwasen Massif reaching an elevation up to 1386 m a.s.l. (Figs. 1 and 2C). The Hochfahrn-Toter Mann Massif demarcates the study area to the north (Fig. 1). At an elevation of 650 m a.s.l., the main valley merges with Buselbachtal into Bruggatal. Further north, this valley leads into Dreisamtal, an east–west-trending tributary valley of the Upper Rhine Graben (Fig. 1).

Quartz-rich lithologies dominate the study area. Gneiss and migmatite are the predominant lithologies on the north-eastern valley wall, whereas paragneisses, migmatite and isolated patches of amphibolites occur on the south-western valley wall as well as in the Katzensteig, Wittenbach and Napf cirques (Hann *et al.*, 2011).

The main valley is one of the most impressive trough valleys in the entire Black Forest (Fig. 2A). The upper part of the main valley is a well-developed stairway cirque with three steps at 1050, 1200 and 1300 m a.s.l. (Fig. 2C; Schreiner, 2011). Morphologically distinct steps separate the Wittenbach and Katzensteig from the main valley (Fig. 2B,C). The upper ends of these hanging valleys are well-developed staircase cirques (Fig. 2B,C). The Katzensteig cirque has two floors at 1020 and 1050 m a.s.l. The tongue basin on the lowermost cirque floor is today occupied by a mire (Fig. 1). The Wittenbach cirque features three individual cirque floors at 990, 1110 and 1170 m a.s.l. (Schreiner, 2011). Further small glacial cirques have been observed on the south-western flank of the main valley NW of the Katzensteig cirque (Fig. 3; Hofmann *et al.*, 2020).

Late Pleistocene glacier fluctuations in the study area

An outlet glacier of both the ice cap on the Feldberg and the ice cap on the summit area of Schauinsland covered almost entirely the study area during the local last glaciation maximum (Fig. 1; Liehl, 1982; Schreiner, 2011; Hemmerle *et al.*, 2016). As previously discussed (Schreiner, 2011; Metz and Saurer, 2012; Hofmann *et al.*, 2020), the glacier front was situated somewhere in Bruggatal (Fig. 1). Its exact location remains unknown, as no terminal moraine has been preserved. The outermost ice-marginal landform in the study area lies on the south-western valley wall at the entrance to the main valley. It is a medial moraine consisting of boulders derived from a glacially transported rockslide ('SW-18' in Fig. 3; Hüttner, 1967; Hofmann *et al.*, 2020).

Multiple terminal moraines have been mapped further upvalley as well as in the tributary valleys. If not explicitly stated otherwise, we refer to the latest study on moraines (Hofmann *et al.*, 2020). A set of moraines (SW-17 to SW-14; Fig. 3C) lies on the NE-facing flank, subparallel to and high above the valley floor (at 900–930 m a.s.l.). The geometry of their crests suggests that the glacier front was located somewhere upvalley from the medial moraine (Fig. 3A). The southernmost of these landforms (SW-14) has an arcuate shape and surrounds a small peat bog. The shape of this moraine indicates that the glacier from the Katzensteig cirque joined the glacier in the main valley during moraine formation (Fig. 3C). A prominent terminal moraine is emplaced at the north-western end of the village of Sankt Wilhelm (SW-13; Figs. 2A and 3C). The double-crested moraine of the ice-marginal positions SW-12 and -11 occupies the area SE of the village (SW-12 and SW-11; Figs. 2A and 3C). The geometry of the crests suggest that the Katzensteig glacier was disconnected from the main valley glacier during moraine formation (Fig. 3C; Schreiner, 2011). A relatively small moraine is positioned further SW (not shown in Fig. 3). At an elevation of about 780 m a.s.l., upvalley from the double-crested moraine, there is a group of arcuate terminal moraines (SW-10 to -8; Fig. 3C). Another moraine is situated 200 m further east (SW-7; Figs. 2A and 3C). The terminal moraine on the southern valley wall 300 m further SE consists almost entirely of boulders (SW-6; Fig. 3C). Two moraines that are only a few metres high lie on the opposite valley wall further upvalley (SW-5 and -4; Fig. 3A). A double-crested terminal moraine is situated at an elevation of 910 m a.s.l (SW-3 and -2; Fig. 3A). The uppermost terminal moraine in the main valley lies on the eastern part of the Napf cirque headwall at an elevation of 1030 m a.s.l. (Fig. 3A).

Multiple moraines are emplaced in the Wittenbach hanging valley (Fig. 3). The northernmost of these progresses from the eastern valley wall in a north-westerly direction down to the bottom of the main valley (Fig. 3A). As the northern end of the ridge is situated on the bottom of the main valley, it is unlikely that the feature is a medial moraine. The landform is rather a terminal moraine of the Wittenbach cirque glacier. Another moraine has been observed at around 950 m a.s.l. on the valley floor. It has a smooth surface and consists of two parts separated by a stream (WB-3; Figs. 2C and 3B). Two moraines are positioned on the eastern valley flank further SW (WB-2 and -1; Fig. 3B). The western moraine leads into an overprinted moraine that surrounds a marshy area on the flat valley floor (WB-1; Fig. 3B). On the western valley flank at an elevation of 1000–1050 m a.s.l., another moraine has been observed (WB-2; Fig. 3B). Further terminal moraines are situated at 1100, 1170 and 1210 m a.s.l. (not shown in Fig. 3).

Numerous moraines have been mapped downvalley from the Katzensteig cirque and in the cirque *sensu strictu*. A

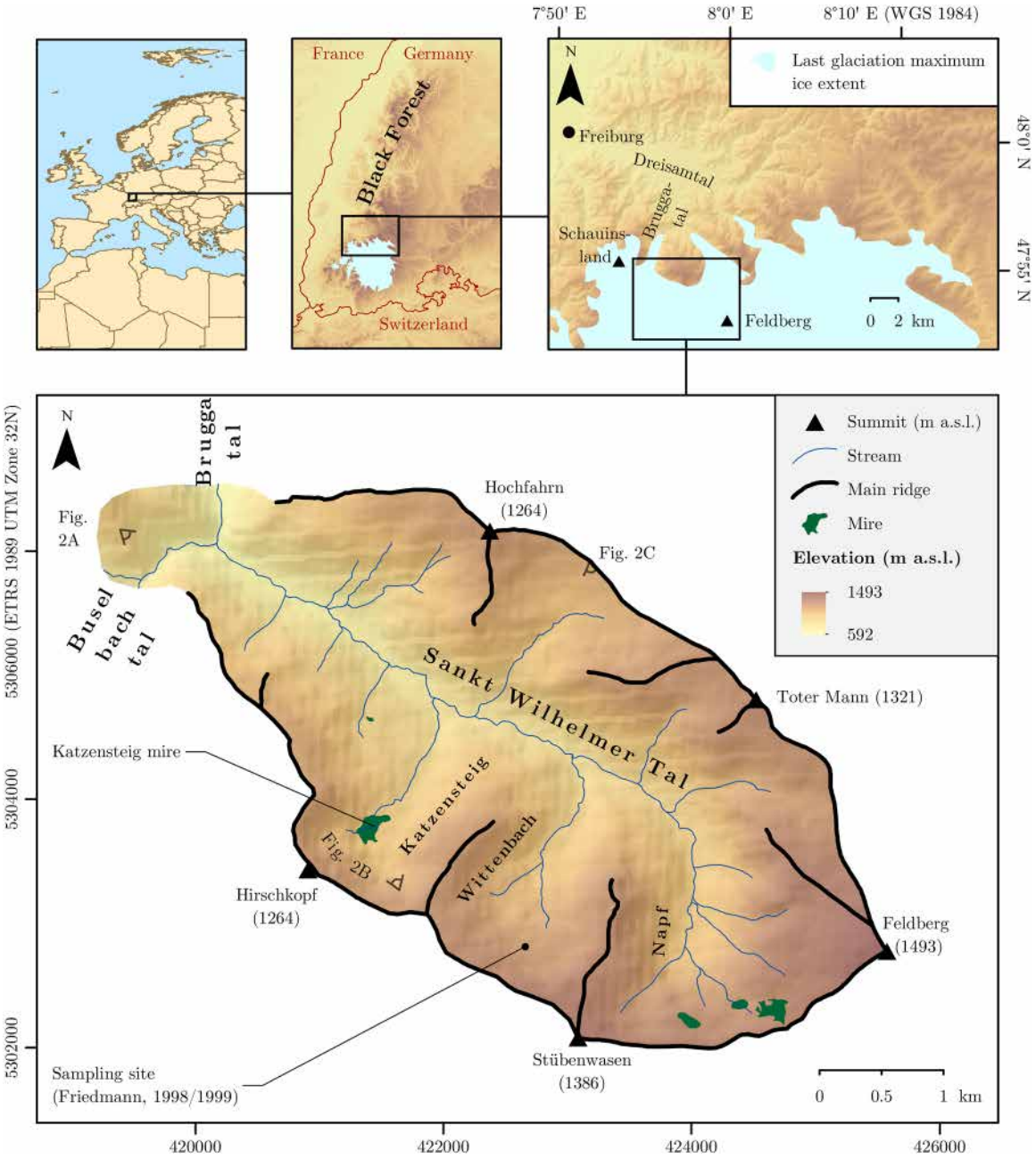

Figure 1. Map of the study area showing mires, the locations where photos were taken for Fig. 2 and localities mentioned in the text. The last glaciation maximum extent in the southern Black Forest is highlighted in light blue (Hemmerle *et al.*, 2016). The shaded relief in the background was derived from a digital terrain model obtained during the SRTM (NASA Jet Propulsion Laboratory, 2013). © EuroGeographics for the administrative boundaries. [Color figure can be viewed at wileyonlinelibrary.com]

smooth moraine has been observed in the area east of the SW-14 sediment ridge (KS-6; Fig. 3C). The mapped moraines further south and SE are subparallel to the valley floor and only up to a few metres high (KS-5 and -4; Fig. 3C). The most prominent terminal moraines are found in the cirque. The northernmost of these (KS-3 and -2) emerge from the western part of the cirque's headwall and surround the well-developed tongue basin on the lowermost cirque floor (Figs. 2B and 3D). A relatively short moraine is found further west (KS-1; Fig. 3D). The upper cirque floor is delimited to the north by an east–west-orientated terminal moraine (KS-1; Figs. 2B and 3D). Multiple moraines are observed on the eastern headwall of the cirque (KS-4 to -7; Figs. 2B and 3D).

Previous investigators (Erb, 1948; Liehl, 1982; Schreiner, 2011) assigned the moraines in the main valley and the tributary valleys to the last deglaciation and proposed that the outlet glacier probably first evolved into a valley glacier and later split into individual cirque glaciers. Due to the lack of chronological data, these moraines were correlated with glacial stades named after groups of terminal moraines NE of Feldberg (cf. Hofmann *et al.*, 2020). As, so far, no attempts have been made to directly date these moraines with modern techniques, these stratigraphic correlations should be considered with caution.

According to data from sediment cores from the Katzensteig mire obtained by the Baden-Württemberg State Institute for the Environment, Survey and Nature Conservation (LUBW), the Laacher See Tephra (deposited at 13 006 ± 9 cal a BP; Reinig *et al.*, 2021) is apparently present slightly above the bottom of the mire (cf. Hofmann *et al.*, 2020). This suggests that the

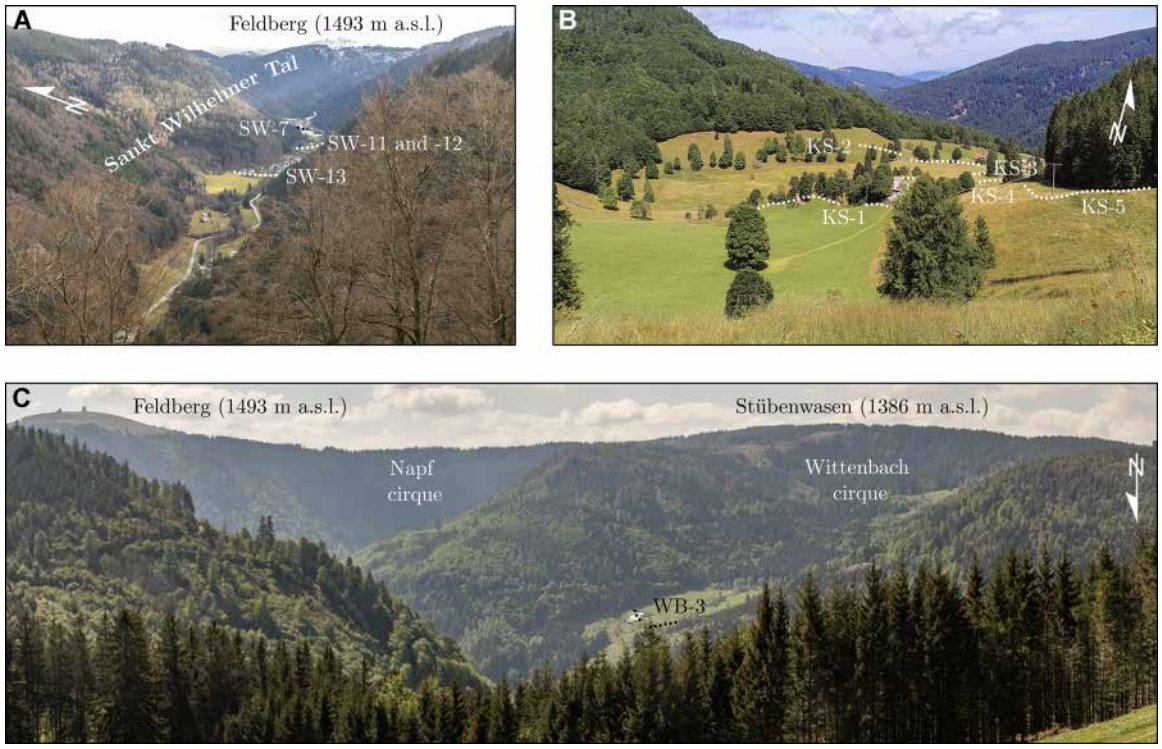

Figure 2. Examples of glacial landforms in the study area. See Fig. 1 for the locations from where the photos were taken. Moraines are highlighted with dotted lines. The numbering refers to the ice-marginal position and starts with the innermost moraine(s) in the cirques. (A) Sankt Wilhelmer Tal and Feldberg seen from the area above the entrance to Sankt Wilhelmer Tal. The valley is one of the most impressive trough valleys in the entire Black Forest. (B) The moraine record in the Katzensteig cirque seen from the cirque's headwall. The upper cirque floor in the foreground is delimited to the north by the terminal moraine of the ice-marginal position KS-1. The smooth moraine of the ice-marginal position KS-5 is situated further east. The tongue basin on the lowermost cirque floor is surrounded by double-crested terminal moraines of the ice-marginal positions KS-2 and -3. The terminal moraine of the ice-marginal position KS-4 is located further uphill. (C) The Wittenbach and Napf stairway cirques seen from the saddle between the Hochfahrn and the Toter Mann. The Wittenbach hanging valley is separated by distinct steps from the main valley. Overprinted terminal moraines (dotted lines) occupy the swampy lowermost floor. The Napf stairway cirque directly leads into the main valley. [Color figure can be viewed at wileyonlinelibrary.com]

terminal moraines at the margin of the mire are at least 13 ka old. A bulk sample from the base of a sediment core from a small mire in the upper part of the Wittenbach cirque (Fig. 1) was dated to 11 110–9904 cal a BP [2σ interval; median probability: 10 462 cal a BP; recalculated from Friedmann (1998/9) with the OxCal software (v. 4.4; Bronk Ramsey, 2009) and IntCal20 (Reimer *et al.*, 2020)]. This radiocarbon age indicates that the upper floors of the Wittenbach cirque were ice-free at the latest at 10.5 ka and that peat formation started at that time.

Methods

Geomorphological mapping and morphostratigraphy

A shaded relief was derived in Esri ArcMap 10.5.1 from a high-resolution digital terrain model (DTM) with an *xy*-resolution of 1 m. Moraines in the study area were mapped in the field with printout versions of the shaded relief (1: 5000 scale). The 'slope' and 'aspect' tools were applied in ArcMap to derive two supplementary raster files for mapping. They were jointly used with scanned field maps. The '3D Analyst' toolbox was used to assess the morphometry of suspected moraines.

Moraines apparently belonging to the same ice-marginal position were then grouped. The following criteria were considered: the geometry of their ends, the size and the elevation on the valley walls. All frontal positions documented by moraines or groups of moraines were then numbered starting with those nearest to the cirques. This allows for adding ice-marginal positions further down the valley in the future, if appropriate.

^{10}Be CRE dating

All sufficiently large and stable moraine boulders were sampled for CRE dating. As it has been shown that CRE ages of tall boulders generally cluster better than those of small boulders (Heyman *et al.*, 2016), only large boulders with a height of more than ~1 m were chosen. To avoid underestimated CRE ages due to boulder toppling and rotating or effects of post-depositional and post-stabilization exhumation, only well-embedded boulders on the crest or distal side of moraines were targeted. As landform stability exerts great influence on CRE age distributions (Tomkins *et al.*, 2021), boulders on matrix-poor and debris-rich moraines were considered particularly suitable.

According to sampling guidelines, flat and horizontal surfaces on moraine boulders should preferably be chosen for CRE dating (Ivy-Ochs and Kober, 2008). As this was often not possible, dipping surfaces with a constant angle were targeted. Rock surfaces near edges were avoided to prevent edge effects (Masarik and Wieler, 2003). A battery-powered saw, a chisel and a hammer were used for sampling. To adjust the ^{10}Be production rate to the sampling sites ($n = 25$; Table 1), the coordinates of the sampling surfaces were determined with a global navigation satellite system (Leica CS20 controller and Leica Viba GS14 antenna). The elevation of the sampling sites was retrieved from the high-resolution DTM mentioned above.

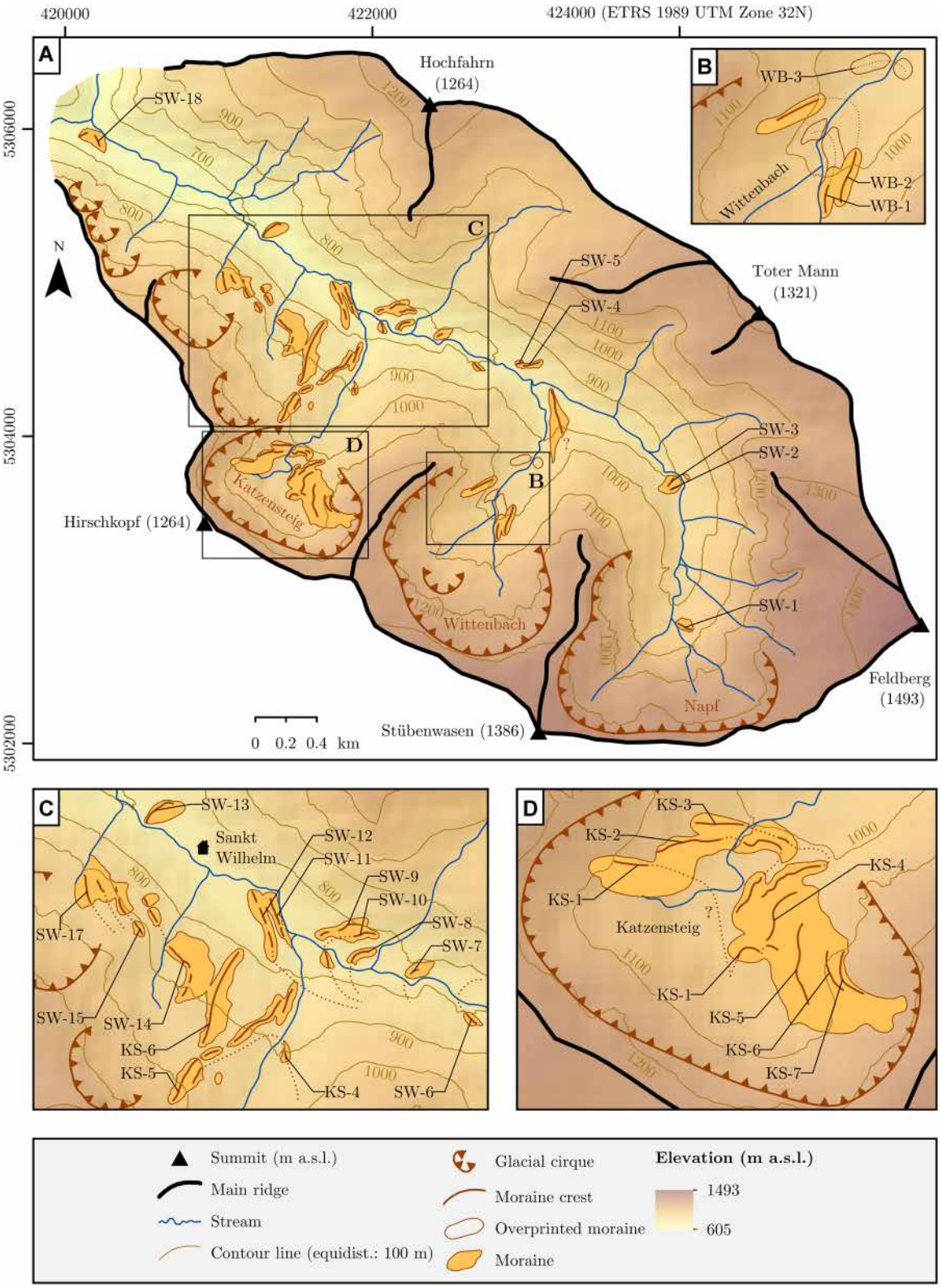

Figure 3. Map of glacial cirques and moraines in (A) the main valley and its tributary valleys, the lower reaches of (B) the Wittenbach hanging valley, (C) the area around the village of Sankt Wilhelm and in (D) the Katzensteig cirque. Inferred ice-margins are marked with dotted lines. See Fig. 1 for the data source of the elevation data in the background. Updated from Hofmann *et al.* (2020). [Color figure can be viewed at wileyonlinelibrary.com]

Pairs of azimuth and elevation angles at the sampling sites were recorded with a handheld SUUNTO inclinometer to determine the topographic shielding factor with an online topographic shielding calculator (Balco, 2018). A dense coniferous forest around the SW-17 boulder prevented us from measuring azimuth and elevation angles. The topographic shielding factor for this sampling site was determined with an ArcGIS toolbox (Li, 2018) and a DTM (*xy*-resolution: about 30 m at the equator) derived from data of the Shuttle Radar Topography Mission (SRTM; NASA Jet Propulsion Laboratory, 2013). As both approaches yielded similar shielding factors for all remaining boulders ($R^2 = 0.93$; $p < 0.01$), those determined with the toolbox of Li (2018) were chosen for ^{10}Be CRE age calculations. The mass and the thickness of the rock fragments in each sample were recorded to compute the mass-weighted average of the sample's thickness for CRE age calculations. A detailed

Table 1. Characteristics of the samples from moraine boulders in Sankt Wilhelmer Tal. The numbering of the samples from the moraine boulders refers to the morphostratigraphical position of the respective terminal moraines

Sample	Latitude (°N WGS 1984)	Longitude (°E WGS 1984)	Elevation (m a.s.l.)	Height above ground of the sampling surface (m)	Lithology	Sample thickness (cm)	Topographic shielding factor
KS-1a	47.880995	7.950002	1039	3.8	Migmatite	1.7	0.970214
KS-1b	47.882771	7.947639	1019	2.5	Migmatite	2.6	0.948215
KS-2a	47.883475	7.948489	1017	1.5	Orthogneiss	1.8	0.960367
KS-2b	47.883464	7.949545	1010	1.4	Orthogneiss	2.1	0.982749
KS-2c	47.883693	7.950439	1011	1.3	Orthogneiss	2.2	0.983238
KS-2d	47.883615	7.950471	1013	1.0	Migmatite	1.9	0.983379
KS-2e	47.883608	7.950357	1013	1.1	Orthogneiss	1.9	0.977940
KS-2f	47.883602	7.948615	1018	1.7	Orthogneiss	2.1	0.973167
KS-2g	47.883334	7.949847	1010	1.8	Orthogneiss	1.8	0.982734
KS-3a	47.883767	7.950995	1006	1.3	Orthogneiss	1.9	0.980652
SW-2	47.882025	7.983656	910	2.9	Migmatite	2.8	0.956313
SW-9	47.891912	7.959058	789	2.1	Migmatite	2.7	0.941004
SW-10	47.891928	7.957121	777	1.1	Migmatite	2.8	0.953857
SW-11a	47.892901	7.954207	759	1.0	Migmatite	2.5	0.967416
SW-11b	47.893093	7.953907	758	1.4	Migmatite	2.7	0.967011
SW-11c	47.893038	7.953808	757	1.7	Migmatite	2.8	0.967081
SW-11d	47.893185	7.953791	755	1.3	Migmatite	2.5	0.927845
SW-12a	47.892540	7.953460	766	1.7	Migmatite	2.4	0.967224
SW-15a	47.891977	7.946590	919	1.5	Migmatite	2.1	0.970717
SW-15b	47.891899	7.946578	919	2.2	Migmatite	2.1	0.963193
SW-16	47.893502	7.944610	916	1.0	Migmatite	2.1	0.984388
SW-17	47.892935	7.943865	934	2.0	Migmatite	2.2	0.958618
SW-18a	47.901610	7.932353	655	1.7	Migmatite	1.9	0.898342
SW-18b	47.901672	7.932376	653	1.8	Migmatite	1.6	0.940309
SW-18c	47.901887	7.931987	654	2.1	Migmatite	1.5	0.880220

sample documentation is provided in the Supporting Information (Appendix S1).

^{10}Be geochemistry

Quartz separation from the rock samples and ^{10}Be extraction from the purified quartz were conducted in the laboratory facilities of the University of Freiburg (Germany) and the Laboratoire National des Nucléides Cosmogéniques (LN_2C) in Aix-en-Provence (France). The separation and purification of quartz follows the procedure outlined in Hofmann *et al.* (2019), with one additional magnetic separation step to further purify the quartz before etching with 48% HF. For this, the acid-leached samples were spiked with magnetic powder and passed through a Frantz magnetic separator.

The ^{10}Be concentrations in the samples were derived from accelerator mass spectrometry (AMS) measurements at the French AMS national facility ASTER (Accélérateur pour les Sciences de la Terre, Environnement, Risques; Arnold *et al.*, 2013) at CEREGE (Centre Européen de Recherche et d'Enseignement des Geosciences de l'Environnement) in Aix-en-Provence (France). During AMS measurements on the KS-2c sample, the ^{9}Be currents were very low, ranging between 0.1 and 0.2 μA. Hence, the ^{10}Be concentration presented below should not be considered reliable and, thus, no CRE age was computed. The measured ^{10}Be/^{9}Be ratios were normalized with respect to the in-house standard STD-11 using an assigned ^{10}Be/^{9}Be ratio of $1.191 \pm 0.013 \times 10^{-11}$ (Braucher *et al.*, 2015) and the Be half-life of $1.387 \pm 0.01 \times 10^{6}$ years (Chmeleff *et al.*, 2010; Korschinek *et al.*, 2010). The ^{10}Be/^{9}Be ratio uncertainty stated in Table 2 comprises the measurement uncertainty (counting statistics), the uncertainty of average standard measures and the systematic error of ASTER (0.5%; Arnold *et al.*, 2010). The ^{10}Be concentrations in the samples were corrected with the ^{10}Be concentration in a batch-specific chemical blank.

Determination of ^{10}Be CRE ages

Apparent ^{10}Be CRE ages were calculated with the online cosmic ray exposure program (CREp; Martin *et al.*, 2017) available at https://crep.otelo.univ-lorraine.fr (last accessed: 1 September 2021). The following parameters were selected: the ^{10}Be production rate deduced from rock samples from the Chironico landslide (southern Switzerland; Claude *et al.*, 2014), which is the closest ^{10}Be production rate reference site to the study area, time-dependent 'Lm' scaling (Nishiizumi *et al.*, 1989; Lal, 1991; Stone, 2000; Balco *et al.*, 2008), the ERA atmosphere model (Uppala *et al.*, 2005), as suggested by Martin *et al.* (2017), and the atmospheric ^{10}Be-based geomagnetic database of Muscheler *et al.* (2005). The assumed spallogenic ^{10}Be production rate amounts to 4.10 ± 0.10 atoms g^{-1} quartz a^{-1} at sea level and high latitudes. As the sampled moraine boulders consist of quartz-rich lithologies, the density of quartz (2.65 g cm^{-3}) was assumed. The CRE ages were not corrected for denudation, vegetation cover or snow shielding.

None of the sampled boulders showed protruding quartz veins. This observation tentatively suggests that postglacial denudation did not significantly affect the sampled boulders. Reuther (2007) inferred a denudation rate (0.24 cm a^{-1}) in a similar setting in the Bavarian Forest (recalculated from Reuther, 2007, with the parameters listed above). Assuming this denudation rate for CRE age calculations would have resulted, on average, in ~2.8% older CRE ages. The CRE age difference amounts to 0.8 ka for the SW-18a boulder with the oldest CRE age, whereas it is negligible for the boulder with the youngest CRE age (10 a). Note that the sampling surfaces on the SW-18a, SW-18b and SW-18c boulders were covered by a few centimetre-thick organic soil. Soils on rock surfaces enhance chemical weathering rates, as they increase the availability of moisture for weathering (Ahnert, 2009). The

Table 2. Results of the ^{10}Be measurements and cosmic-ray exposure (CRE) ages of sampled boulders in the Katzensteig cirque (KS) and in Sankt Wilhelmer Tal *sensu strictu* (SW). The ^{10}Be concentrations in the samples were corrected with the ^{10}Be concentration in a batch-specific chemical blank

Sample	Mass of dissolved quartz (g)	^{9}Be-spike added ($\times10^{19}$ atoms)	^{10}Be/^{9}Be ratio ($\times10^{-14}$)	^{10}Be concentration and uncertainty (atoms g^{-1} quartz)	^{10}Be CRE age (ka)*
KS-1a	15.1849	2.98011	7.055 ± 0.230	135 710 ± 4430	14.26 ± 0.56 (0.45)
KS-1b	6.4533	3.04459	0.929 ± 0.084	37 328 ± 3383	4.30 ± 0.39 (0.38)
KS-2a	18.8670	3.07734	6.022 ± 0.270	96 000 ± 4312	10.45 ± 0.51 (0.45)
KS-2b	11.7265	3.05975	4.773 ± 0.218	120 961 ± 5538	12.91 ± 0.66 (0.58)
KS-2c	5.4448	2.99527	3.360 ± 0.741	177 138 ± 39 079†	13.52 ± 0.66 (0.58)
KS-2d	19.7940	3.07168	8.346 ± 0.364	127 408 ± 5563	13.52 ± 0.66 (0.58)
KS-2e	14.8645	3.08482	6.837 ± 0.264	139 080 ± 5377	14.79 ± 0.65 (0.55)
KS-2f	11.6719	3.08765	3.198 ± 0.179	81 010 ± 4542	8.75 ± 0.51 (0.47)
KS-2g	12.7346	3.08563	4.823 ± 0.228	113 582 ± 5388	12.10 ± 0.63 (0.56)
KS-3a	14.5545	3.09856	6.304 ± 0.279	131 342 ± 5817	14.04 ± 0.68 (0.60)
SW-2	9.7627	3.09573	3.826 ± 0.212	117 041 ± 6488	13.99 ± 0.82 (0.75)
SW-9	10.9071	3.11029	4.358 ± 0.179	120 427 ± 4956	16.11 ± 0.74 (0.64)
SW-10	15.0384	3.09452	5.968 ± 0.313	120 033 ± 6301	16.01 ± 0.89 (0.81)
SW-11a	8.1310	3.07673	3.600 ± 0.194	131 076 ± 7076	17.43 ± 1.00 (0.91)
SW-11b	15.9217	3.11170	3.874 ± 0.159	73 090 ± 3015	9.88 ± 0.46 (0.39)
SW-11c	6.4325	3.09775	2.467 ± 0.123	112 323 ± 5630	15.06 ± 0.81 (0.73)
SW-11d	8.4611	3.07067	3.602 ± 0.189	125 784 ± 6620	17.50 ± 0.98 (0.89)
SW-12a	9.4630	3.09270	4.064 ± 0.146	128 392 ± 4626	16.98 ± 0.71 (0.60)
SW-15a	10.4747	3.05611	4.991 ± 0.188	141 626 ± 5347	16.38 ± 0.71 (0.60)
SW-15b	22.7848	3.08906	11.251 ± 0.357	150 706 ± 4801	17.54 ± 0.68 (0.54)
SW-16	13.6787	3.07228	1.428 ± 0.127	29 022 ± 2591	3.51 ± 0.32 (0.31)
SW-17	11.1192	3.05268	5.271 ± 0.188	140 959 ± 5047	16.33 ± 0.68 (0.56)
SW-18a	17.1210	3.08664	7.226 ± 0.330	127 834 ± 5852	19.85 ± 0.99 (0.88)
SW-18b	19.6887	3.08563	7.641 ± 0.284	117 627 ± 4389	17.49 ± 0.76 (0.63)
SW-18c	20.6816	3.07370	7.289 ± 0.303	106 304 ± 4431	16.87 ± 0.79 (0.68)

*CRE age uncertainties comprise both 1σ analytical uncertainties (internal uncertainty) and the error associated with the ^{10}Be production rate. Internal uncertainties are presented in parentheses.

†During AMS measurements on the KS-2c sample, the ^{9}Be currents only ranged between 0.1 and 0.2 μA. Hence, the ^{10}Be concentration may be out of the 1σ range, and it should not be considered reliable. Thus, no CRE age was computed.

sampled soil-covered boulders may have experienced even stronger postglacial denudation.

The boulders on the moraines of the ice-marginal positions SW-2, -15, -16, -17 and -18 in the main valley lie in forested areas. Vegetation cover alters the ^{10}Be production rate by a few per cent (e.g. Kubik *et al.*, 1998). Reuther *et al.* (2011) incorporated the effect of vegetation cover on CRE ages of boulders with biomass estimates. She had already noted that the effect on the resulting CRE ages is rather small (about 4%; Reuther, 2007). Even in extreme cases, such as trees growing on top of boulders, CRE ages did not change significantly. The sampling surfaces on the SW-18a, SW-18b and SW-18b boulders were covered by an about 5-cm-thick organic soil and lichen which may have additionally slowed down the accumulation of *in situ* produced ^{10}Be.

According to field observations in 2021 (with a rather cool spring and summer in the region), the sampled boulders in the Katzensteig and Napf cirques as well as in the main valley were covered by a several decimetre-thick snow cover in winter. The sampled boulders are not located in windswept areas where snow drift exposes their surfaces. According to data of the German Weather Service (DWD) from the weather station at Titisee (850 m a.s.l.), located several kilometres NE of the study area, snow cover lasted, on average, for 4 months per year in the 1961–1990 period. Average snow cover amounted to about 30 cm. Assuming a similar snow cover on top of the sampled boulders, a snow density of 0.3 g cm^{-3}, an attenuation length for fast neutrons in snow of 109 g cm^{-2} (Zweck *et al.*, 2013), the commonly used equation 3.76 in Gosse and Phillips (2001) yields a snow shielding factor of ~0.97. Incorporating this factor would yield ~2.6% older CRE ages. The climate in the Alps and their forelands strongly varied during the duration of exposure (see Heiri *et al.*, 2014, and references therein), thus raising the question of whether snow cover in the period 1961–1990 is representative. We conclude that the CRE ages presented below may be underestimated by a few hundred years.

Computation of landform ages

Multiple boulders were sampled per terminal moraine, if possible, to allow for detecting potentially underestimated and overestimated CRE ages. The assessment of the CRE ages follows the procedure in version 3 of the online calculator formerly known as the CRONUS-Earth online calculator (Balco *et al.*, 2008). See Balco (2017) for further details.

Reduced chi-squared (χ^2_R) statistic was first performed for sets of at least three CRE ages. This test allows for determining whether the variation of the CRE ages from the same landform is predominantly caused by analytical uncertainties ($\chi^2_R \approx 1$) or by geomorphological factors, such as post-depositional exposure ($\chi^2_R \gg 1$). Reduced chi-squared is then compared with a critical value from a standard χ^2-table, whereby the degree of freedom is $n-1$. In this study, the confidence interval was set to 95%. The critical value is then divided by the degrees of freedom. If χ^2_R is lower than this value, the hypothesis that the data form a single population cannot be excluded at 95% confidence. A higher χ^2_R implies that measurement uncertainties do not fully account for the scatter in the CRE ages (Balco, 2011).

For sets of CRE ages from terminal moraines yielding a χ^2_R lower than the critical value, the arithmetic mean CRE age was chosen as the landform age. Its uncertainty was calculated by adding the average analytical uncertainty and the ^{10}Be-production

rate error in quadrature, as done elsewhere (e.g. Le Roy *et al.*, 2017). If χ^2_R turned out to be higher than the critical value, the CRE age with the worst χ^2_R was considered an outlier. This procedure was repeated until the remaining CRE ages yielded an acceptable χ^2_R value. Not more than half of the CRE ages from the same landform were removed.

Recalculation of ^{10}Be CRE ages from key moraine records in Central Europe

To allow for pertinent comparison, 83 previously published ^{10}Be CRE ages for key sites in mountainous regions in Central Europe and their forelands were recalculated (Tables S1 and S2). As the climate south of the main weather divide in the Alps differs substantially from the climate further north (Glaser *et al.*, 2013), the area of interest was restricted to the region north and NE of the main weather divide.

All necessary data for recalculation of the ^{10}Be CRE ages were either retrieved from the original publications or obtained from the authors. Outliers were excluded as suggested by the authors. Recalculation of the ^{10}Be CRE ages was performed in the CREp calculator with the same parameters listed above. This calculator requires ^{10}Be concentrations computed with the 07KNSTD standardization as input (Martin *et al.*, 2017). As most of the previously published ^{10}Be concentrations were determined with other standardizations, they were first recalculated with appropriate conversion factors. These were retrieved from a MATLAB script of version 2.3 of the online exposure age calculator, formerly known as the CRONUS-Earth online exposure age calculator (make_al_be_consts_v23.m; Balco, 2007). If topographic shielding factors were not reported in the original publications, they were determined with an SRTM-DTM (*xy*-resolution: about 30 m at the equator; NASA Jet Propulsion Laboratory, 2013) and the ESRI ArcGIS toolbox of Li (2018). The ages were not corrected for snow cover and postglacial denudation.

Glacier and ELA reconstructions

The ELA is commonly defined as the zones of a glacier where the mass balance is zero on an annual timescale (Bakke and Nesje, 2011). Reconstructing ELAs reveals palaeoclimatic information if factors other than climate do not significantly influence its position (Mackintosh *et al.*, 2017). ELAs are also used as a tool for stratigraphic correlations of terminal moraines at the local scale when topographic and lithological conditions are similar (Reitner *et al.*, 2016).

The aim of the ELA reconstructions for this study was two-fold: first, we aimed to evaluate whether ELA reconstructions are a suitable tool for relative dating of moraines in the southern Black Forest. Finding an appropriate relative dating technique is of particular interest for future studies, since the lack of suitable boulders hampered CRE dating of the terminal moraines in the Wittenbach hanging valley and will certainly be an obstacle in future studies. ELA reconstructions could be one potential way to circumvent this issue. Several observations suggest similar ELAs in the Napf, Wittenbach and Katzensteig cirques at the same time. These cirques are orientated towards the NE, the cirques' morphology is very similar, as they feature steep western and gently sloping eastern headwalls, and the same bedrock lithologies occur in all cirques. Potentially existing factors other than climate should thus influence the position of the ELA in a similar way. ELA reconstructions should yield similar ELAs for moraines with the same ^{10}Be CRE age. Second, determining ELAs during moraine formation provides the opportunity for future reconstructions of palaeo-precipitation in the southern Black Forest.

The two ELA reconstruction approaches selected for this study, the accumulation area ratio (AAR) and area–altitude balance ratio (AABR) methods, require glacier surface reconstructions which were performed with the GlaRe ArcGIS toolbox (Pellitero *et al.*, 2016). For the first step, the flowlines of the glaciers in the study area were created as shapefiles in ArcMap 10.5.1. Points with a spacing of 50 m at the flowlines were subsequently created using the 'interval nodes' tool in GlaRe. The 'flowline ice thickness' tool enabled the ice surface elevation at these points to be calculated. This tool requires the basal shear stress as primary input. Thanks to the presence of terminal moraines, reconstruction of the ice margin near the glacier fronts turned out to be straightforward. As suggested (Pellitero *et al.*, 2016), the shear stress was progressively adjusted to make the reconstructed ice thickness fit to these landforms. However, this was not possible further up the glaciers due to the lack of landforms indicative of former ice margins. Thus, the default shear stress of 100 000 Pa in the GlaRe toolbox was assumed in these areas. This is a reasonable assumption, as the basal shear stress beneath glaciers normally varies between 50 000 and 100 000 Pa (Paterson, 1994). Nevertheless, the variation of previously published shear stress values is large and even higher basal shear stress values have been reported (Paterson, 1970; Boulton *et al.*, 1979; Cohen *et al.*, 2000). The choice of the basal shear stress is thus considered the major source of uncertainty in our glacier reconstructions. Since it is unrealistic that the driving stress of topographically constrained glaciers is entirely supported by the basal shear stress (Benn and Hulton, 2010), the ice thickness at points along glacier flowlines in topographically constrained areas was recalculated by incorporating a dimensionless shape factor (*f*). It was derived from automatically created cross-sections using the 'automatic ice thickness recalculation with f factor' tool in GlaRe.

For the next step, contour lines of today's surface were derived from a high-resolution DTM with an *xy*-resolution of 5 m. Glacier contours were drawn from the interval nodes to the contour lines of today's surface according to the ice surface elevation at the interval nodes. Following the approach introduced by Sissons (1974), convex and concave contour lines were drawn in the suspected ablation and accumulation areas of the glaciers, respectively. The contour lines were transformed into digital elevation models (DEMs) of the glaciers by applying the 'from contour to DEM' tool in the ArcGIS ELA calculation toolbox of Pellitero *et al.* (2015).

ELAs in the Alps have traditionally been determined with the surface reconstruction method, which assumes a fixed proportion between the accumulation and ablation areas of a glacier (Pellitero *et al.*, 2015). Gross *et al.* (1977) found that an AAR of 0.67 is appropriate for glaciers in the European Alps. Kern and László (2010) later showed that this value is only appropriate for larger glaciers and that smaller AARs are sufficient to keep small glaciers in a steady state. We argue that the glaciers in the Alps in their dataset are probably the best analogues for the former glaciers in the study area. Based on the data presented in Kern and László (2010), the following equation was established for selecting suitable AARs for the reconstructed glaciers:

$$AAR = 0.108*\ln(s) + 0.4567 \quad (1)$$

where s is the surface of the glacier (km^2). We assume that the error of the AARs calculated with Equation (1) does not depend on the size. Thus, the differences between the actual AARs and the AARs derived with Equation (1) was computed for every glacier in the Alps included in the study of Kern and László (2010). The standard deviation of these values (0.056) was

considered the AAR uncertainty. AAR-ELAs were determined with the ArcGIS toolbox of Pellitero *et al.* (2015).

The AAR method has been heavily criticized, as it neglects the hypsometry of a glacier which may significantly influence the position of the ELA (Pearce *et al.*, 2017). In contrast, the AABR method explicitly takes this factor into account (Rea, 2009). Rea (2009) published a large global dataset with AABRs. To ensure comparability with the ELAs derived with the AAR method, we chose the mean AABR for the European Alps (1.59) derived from data of 12 glaciers. However, as mentioned by Boston *et al.* (2015), most of them were in retreat, which may induce errors in ELA reconstructions. To take the high variation of the balance ratios of the glaciers in the Alps into account ($1\sigma = 0.59$), each balance ratio from the Alps was used to compute the ELA with the toolbox of Pellitero *et al.* (2015). The contour line interval was set to 10 m during ELA calculations and, thus, the ELA uncertainty is 5 m (Pellitero *et al.*, 2015). The standard deviation of the ELAs computed for each glacier was considered the ELA uncertainty. The error of the ELA calculation toolbox was added in quadrature.

Results and interpretation

Mapping of moraines

A detailed geomorphological map of the study area has already been published (Hofmann *et al.*, 2020). Therefore, we only present changes in light of new field evidence. An updated map of terminal moraines and ice-marginal positions in the study area is given in Fig. 3.

Field mapping of the area around the double-crested moraine of the ice-marginal positions SW-11 and -12 revealed that there is not a distinct sediment ridge uphill from the double-crested moraine. Rather, the moraine's outer crest is overlain by a cone-shaped hump. Due to the positioning on the moraine crest and shape of the feature, we propose that the landform was emplaced during a mass movement after moraine formation. Hence, the hump should not be classified as a terminal moraine, as done in previous work (Hofmann *et al.*, 2020). As outcropping bedrock was observed at previously mentioned moraines upvalley from the lowermost floor of the Wittenbach cirque (Hofmann *et al.*, 2020), these landforms should not be classified as terminal moraines.

Overall, moraines of 18 ice-marginal positions have been mapped in the main valley. Moraines of multiple ice-marginal positions are found in the Wittenbach and Katzensteig hanging valleys (Fig. 3).

^{10}Be CRE ages

Apparent CRE ages of the sampled moraine boulders in ka (thousand years before 2010 CE) are given in Fig. 4 as well as in Table 2. For landform ages, i.e. CRE ages of terminal moraines as well as χ^2_R values, see Table 3.

Three boulders on the SW-18 moraine yielded ages between 19.9 ± 1.0 and 16.9 ± 0.8 ka. As χ^2_R (4.03) exceeded the critical value, the age of the SW-18a boulder with the worst χ^2_R was considered an outlier. The two remaining ages led to a landform age of 17.2 ± 0.8 ka. Only one boulder on the proximal side of the terminal moraine of the ice-marginal position SW-17 proved to be a suitable candidate for ^{10}Be CRE dating and yielded an age of 16.3 ± 0.7 ka. CRE dating of the only sufficiently large boulder on the SW-16 moraine resulted in a considerably younger age of 3.5 ± 0.3 ka. Two boulders on the moraine of the ice-marginal position 15 (SW-15a and SW-15b) gave ages of 16.4 ± 0.7 and 17.5 ± 0.7 ka, respectively, resulting in a landform age of 17.0 ± 0.7 ka. The lack of suitable boulders prevented sampling of the SW-14 and -13 moraines. Boulder SW-12a from the ice-marginal position SW-12 was dated to 17.0 ± 0.7 ka. The SW-11a boulder from the ice-marginal position SW-11 has an age of 17.4 ± 0.9 ka, whereas boulders SW-11b, SW-11c and SW-11d on the moraine's distal side gave ages of 9.9 ± 0.5, 15.1 ± 0.8 and 17.5 ± 1.0 ka, respectively. The youngest ages from the SW-11b and SW-11c boulders were classified as outliers, resulting in a landform age of 17.5 ± 1.0 ka.

Only one sufficiently large boulder for CRE dating was situated on the SW-10 moraine, yielding a CRE age of 16.0 ± 0.9 ka. A boulder on the morphostratigraphically next oldest moraine gave an indistinguishable age (16.1 ± 0.7 ka). Sufficiently large and stable boulders did not occur on the moraines of the ice-marginal positions SW-7 to -4. The SW-2 boulder on the inner crest of the double-crested terminal moraine further upvalley (ice-marginal position SW-2) was dated to 14.0 ± 0.8 ka. Due to the lack of suitable boulders, the SW-1 moraine was not sampled.

CRE dating was not applied to terminal moraines in the Wittenbach valley and stairway cirque, as only one sufficiently large and stable moraine boulder was recognized during a field survey.

The only sampled boulder on the distal side of the double-crested moraine of the ice-marginal position KS-3 in the Katzensteig cirque was dated to 14.0 ± 0.7 ka. The ages of six sampled boulders on the inner crest of the moraine and on its proximal side range from 8.8 ± 0.5 to 14.8 ± 0.7 ka. Since χ^2_R (19.18) considerably exceeded the critical value, the ages of boulders KS-2a, KS-2e and KS-2f were discarded, as they yielded the worst χ^2_R. The landform age of 12.8 ± 0.7 ka corresponds to the average of the remaining ages. Boulders KS-1a and KS-1b yielded two differing ages (14.3 ± 0.6 and 4.3 ± 0.4 ka).

Interpretation of ^{10}Be CRE ages

Considering CRE age uncertainties, the CRE ages presented here are consistent with the morphostratigraphy apart from a few outliers. This study demonstrates that CRE dating is a suitable technique for reconstructing glacier variations in anthropogenically modified environments where the number of suitable boulders is limited.

Geomorphological field evidence suggests that post-depositional processes probably did not affect the sampled boulders on the SW-18 moraine. As the moraine consists almost entirely of boulders, boulder toppling and rotating as well as post-depositional exhumation seem highly unlikely. The consistent CRE ages of boulders SW-18b and SW-18c are thus deemed robust. Pre-exposure to secondary cosmic radiation is the most likely explanation for the outlying CRE age of the SW-18a boulder, as the moraine's sediments probably originate from a rockslide. Since the boulders are partly rounded, we argue that they were transported to their present location by an advancing glacier. The SW-18a boulder may thus have experienced pre-exposure. Recent studies on rockslides demonstrate that the ^{10}Be CRE ages of boulders may largely exceed the age of the failure (e.g. Hilger *et al.*, 2019).

Apart from the CRE ages of the SW-16, SW-11b and SW-11c boulders, the ages from the ice-marginal positions SW-17 to -2 are consistent with the morphostratigraphy. The age of the SW-16 boulder is considered an outlier. As this boulder is situated on the steep proximal side of the moraine, it may have undergone displacement or toppling. Weathering and spalling may have also affected the sampling surface, as the boulder only has a thin moss cover when compared to the boulders on

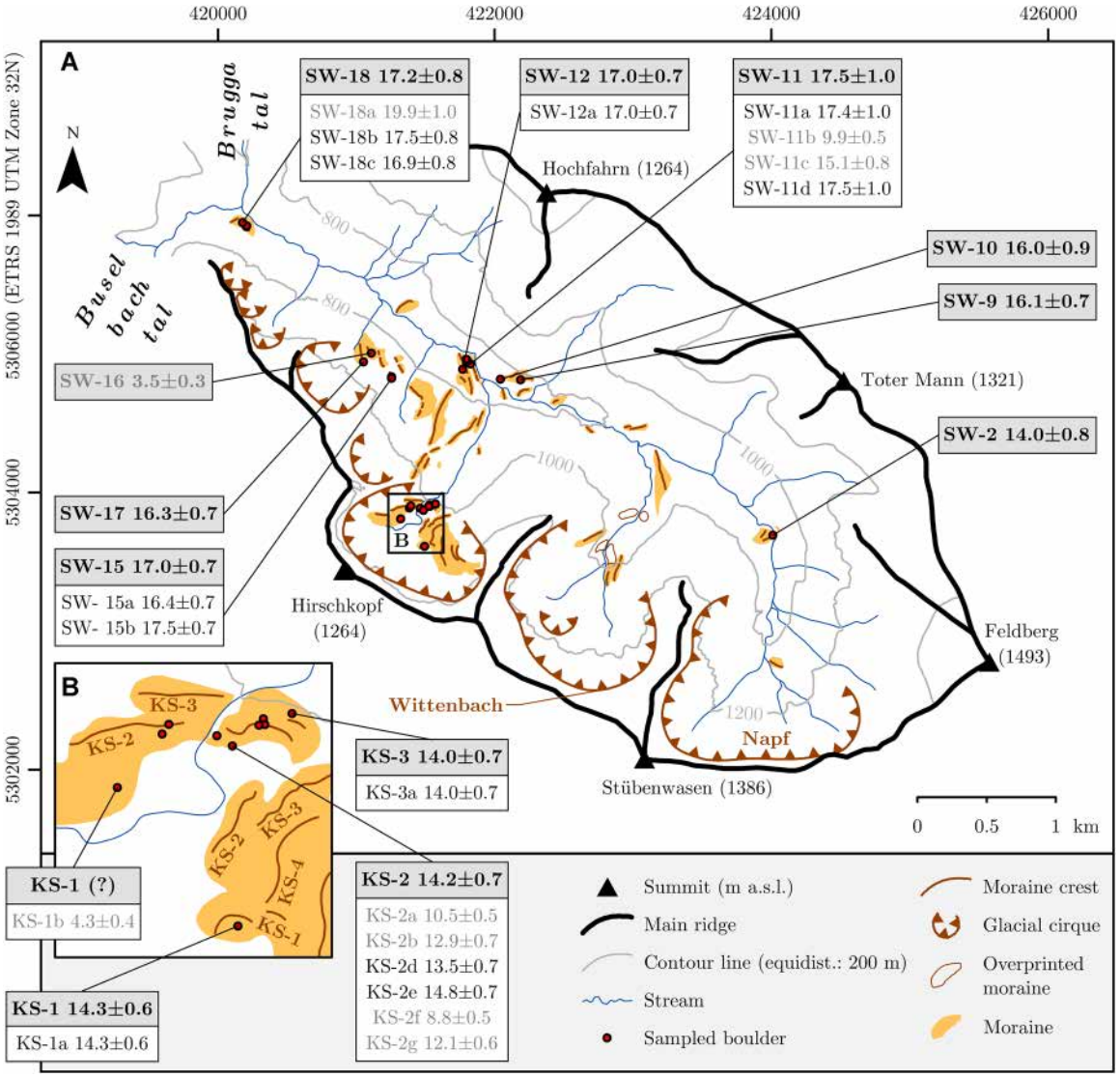

Figure 4. Glacial cirques, moraines and sampled moraine boulders in (A) the whole study area and (B) the Katzensteig cirque. The ^{10}Be CRE ages of the moraine boulders in ka (thousand years before 2010 CE) and the external uncertainties are presented in white boxes. Landform ages are given in grey boxes. Outlying CRE ages are shown in grey. [Color figure can be viewed at wileyonlinelibrary.com]

the moraine of the ice-marginal positions SW-15 and -17 (Appendix S1). As the SW-11b boulder is very angular (Appendix S1), the outlying CRE age of this boulder may be explained by spalling.

The age of the KS-3a boulder is deemed robust, as the boulder is well embedded in the moraine and sufficiently large. The CRE age of the ice-marginal position KS-2 (12.8 ± 0.7 ka) is not considered meaningful. Indeed, the CRE age of the exceptionally large boulder on a moraine of the ice-marginal position KS-1 indicates that this moraine formed not later than 14.3 ± 0.6 ka. Hence, the moraines of the ice-marginal position KS-2 must be at least 14.3 ± 0.7 ka old. Only the CRE ages of the SW-2d and KS-2e boulders are consistent with the morphostratigraphy and, thus, the arithmetic mean CRE age of these boulders (14.2 ± 0.7 ka) is considered the landform age (Fig. 4B). Although the sampling surfaces on boulders KS-2a, KS-2b, KS-2f and KS-2g were considered undisturbed during fieldwork, the sampling surfaces may have been altered by post-depositional processes, such as weathering or spalling. It should also be kept in mind that the boulders are situated in a landscape which has significantly been modified by human activity. The CRE age of the KS-1a boulder is considered particularly robust, as the boulder is, by far, the largest sampled. The outlying CRE age of the KS-1b boulder may be explained by postglacial weathering.

ELAs during moraine formation

Reconstructed ELAs are presented in Table 4; see also Figs. 5–7. As explained above, ELAs determined with the AABR method are considered more robust. Hence, we only comment on them in the following paragraphs. AAR-ELAs are given in parentheses.

As the position of the glacier front in Bruggatal during the emplacement of the SW-18 moraine remains unknown, the ELA during moraine formation could not be reconstructed. The determination of ELAs during the formation of the terminal moraines of the ice-marginal positions SW-17 to -14 proved impossible for the same reason.

Two scenarios were tested for the well-developed terminal moraine of the ice-marginal position SW-13: according to the first scenario, the landform formed in front of a combined glacier from the Napf, Katzensteig and Wittenbach cirques. This glacier would have had an ELA of 1107 ± 22 m a.s.l. (1062–1112 m a.s.l.). Liehl (1982) hypothesized that the glacier from the Katzensteig cirque did not feed any more

Table 3. ^{10}Be CRE ages of terminal moraines in Sankt Wilhelmer Tal and in the Katzensteig cirque

Location	Ice-marginal position	Number of CRE ages	Landform age and uncertainty (ka) after the exclusion of outliers	Reduced χ^2
Katzensteig cirque (KS)	KS-1	2	14.3 ± 0.6	–
	KS-2	6	14.2 ± 0.7*	19.18
	KS-3	1	14.0 ± 0.7	–
Sankt Wilhelmer Tal (SW)	SW-2	1	14.0 ± 0.8	–
	SW-9	1	16.1 ± 0.7	–
	SW-10	1	16.0 ± 0.9	–
	SW-11	4	17.5 ± 1.0	61.87
	SW-12	1	17.0 ± 0.7	–
	SW-15	2	17.0 ± 0.7	–
	SW-16	1	-†	–
	SW-17	1	16.3 ± 0.7	–
	SW-18	3	17.2 ± 0.8	4.03

*As the CRE age of the KS-1a boulder suggests that the KS-2 moraine has a minimum age of 14.3 ± 0.6 ka, the landform age corresponds to the average CRE ages of the KS-2d and KS-2e boulders. All other CRE ages from the KS-2 moraine were considered outliers.

†Since the landform ages of the SW-15 and SW-17 moraines indicate that the SW-16 moraine formed between 16.3 ± 0.7 and 17.0 ± 0.7 ka, the only CRE age from the SW-17 moraine (3.5 ± 0.3 ka) is considered largely underestimated.

the main valley glacier at this time. In this scenario the ELA would have been 1106 ± 24 m a.s.l. (1061–1131 m a.s.l.).

The ELA was 1127 ± 19 m a.s.l. (1082–1152 m a.s.l.) when the double-crested terminal moraine of the ice-marginal positions SW-12 and -11 formed. With 1126 ± 19 m a.s.l. (1091–1161 m a.s.l.), the ELA remained almost unchanged during deposition of the terminal moraines of the ice-marginal positions SW-10 and -9 as well as during emplacement of the moraine of the ice-marginal position SW-8 (1125 ± 19 m a.s.l.; 1100–1160 m a.s.l.). The equilibrium line was situated at a slightly higher elevation (1136 ± 19 m a.s.l.) when the terminal moraine of the ice-marginal position SW-7 formed (AAR-ELA: 1111–1161 m a.s.l.). An ELA of 1134 ± 21 m a.s.l. (1119–1169 m a.s.l.) was reconstructed for the ice-marginal position SW-6. With 1143 ± 19 m a.s.l. (1118–1178 m a.s.l.), the ELA remained similar during emplacement of the terminal moraines of the ice-marginal positions SW-5 and -4.

The Napf cirque glacier had an equilibrium line at a significantly higher elevation (1195 ± 17 m a.s.l.; AAR-ELA: 1230–1290 m a.s.l.) during formation of the double-crested terminal moraine of the ice-marginal positions SW-3 and -2. The ELA was 1268 ± 13 m a.s.l. (1313–1343 m a.s.l.) when the terminal moraines of the ice-marginal position SW-1 formed.

If the terminal moraine at the entrance to the Wittenbach hanging valley pertains to the Wittenbach cirque glacier, the ELA must have been 1133 ± 19 m a.s.l. (1188–1228 m a.s.l.). Under the assumption that the feature formed at the glacier from the Napf cirque, the ELA was 1145 ± 18 m a.s.l. (1140–1190 m a.s.l.). The equilibrium line was situated at an elevation of 1178 ± 15 m a.s.l. (1213–1253 m a.s.l.) during formation of the overprinted terminal moraine of the ice-marginal position WB-3. Similar ELAs (1195 ± 11 and 1196 ± 11 m a.s.l.; AAR-ELAs: 1231–1261 and 1230–1260 m a.s.l.) were reconstructed for the moraines of the ice-marginal positions WB-2 and -1.

When the terminal moraines of the ice-marginal position KS-5 of the Katzensteig glacier formed, the ELA was probably 1076 ± 18 m a.s.l. (1131–1171 m a.s.l.). The glacier had an ELA of 1097 ± 15 m a.s.l. (1152–1192 m a.s.l.) during the emplacement of the terminal moraines of the ice-marginal position KS-4. During formation of the moraines of the ice-marginal positions KS-3 and -2, the equilibrium line of the Katzensteig cirque glacier was situated at 1145 ± 10 m a.s.l. (1180–1210 m a.s.l.). A similar ELA (1145 ± 9 m a.s.l.; AAR-ELA: 1180–1210 m a.s.l.) was reconstructed for the ice-marginal position KS-1.

Table 4. Reconstructed equilibrium line altitudes (ELAs) during ice-marginal positions in Sankt Wilhelmer Tal as well as in the Wittenbach and Katzensteig hanging valleys. ELAs were determined with both the area–altitude balance ratio (AABR) and accumulation area ratio (AAR) method. The AABR-ELAs were computed with a balance ratio of 1.59. ELA uncertainties were determined as follows: the ELA during the ice-marginal positions was determined with 12 balance ratios of glaciers in the Alps (see Rea, 2009). The standard deviation of the ELAs was then derived. The uncertainty of each ELA (5 m) was added in quadrature

Location	Ice-marginal position		AABR-ELA (m a.s.l.)	AAR-ELA (range; m a.s.l.)
Sankt Wilhelmer Tal (SW)		SW-1	1268 ± 13	1328 (1313–1343)
		SW-2 and -3	1195 ± 17	1255 (1230–1290)
		SW-4 and -5	1143 ± 19	1143 (1118–1178)
		SW-6	1134 ± 21	1144 (1119–1169)
		SW-7	1136 ± 19	1136 (1111–1161)
		SW-8	1125 ± 19	1135 (1100–1160)
		SW-9 and -10	1126 ± 19	1126 (1091–1161)
		SW-11 and -12	1127 ± 19	1117 (1082–1152)
	SW-13	Scenario 1 (combined Napf and Wittenbach glacier)	1106 ± 24	1096 (1061–1131)
		Scenario 2 (combined Katzensteig, Wittenbach and Napf glacier)	1107 ± 22	1087 (1062–1112)
Wittenbach (WB)		WB-1	1195 ± 11	1245 (1230–1260)
		WB-2	1196 ± 11	1246 (1231–1261)
		WB-3	1178 ± 15	1238 (1213–1253)
	WB-4 (?)	Scenario 1 (Wittenbach glacier)	1133 ± 19	1213 (1188–1228)
		Scenario 2 (Napf glacier)	1145 ± 18	1175 (1140–1190)
Katzensteig (KS)		KS-1	1145 ± 9	1195 (1180–1210)
		KS-3	1145 ± 10	1195 (1180–1210)
		KS-4	1097 ± 15	1167 (1152–1192)
		KS-5	1076 ± 18	1146 (1131–1171)

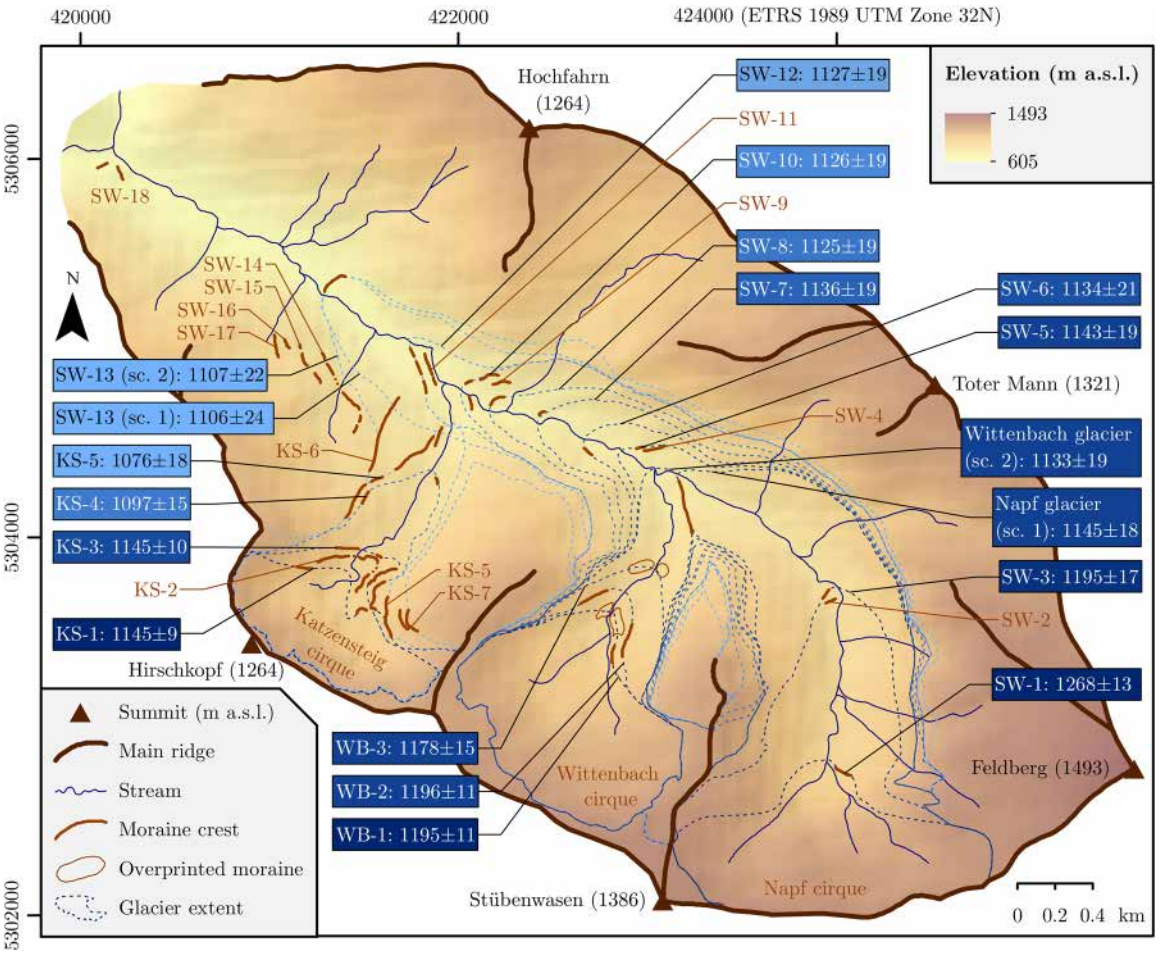

Figure 5. Reconstructed glacier extents and AABR-ELAs (m a.s.l.) during moraine formation. Two scenarios were tested for the moraine of the ice-marginal position SW-13: according to the first scenario (sc. 1), the moraine formed at the front of a combined glacier from the Wittenbach and Napf cirques. In the second scenario (sc. 2) the glacier from the Katzensteig cirque still joined the main valley glacier. See Fig. 1 for the data source of the shaded relief in the background. [Color figure can be viewed at wileyonlinelibrary.com]

Discussion

Late Pleistocene glacial history of the study area

The moraine of the outermost securely identified ice-marginal position (SW-18) formed no later than ~17 ka. Overlapping CRE ages suggest that emplacement of the moraines of the ice-marginal positions SW-17, −16 and -15 probably occurred shortly thereafter.

As the terminal moraine of the ice-marginal position SW-13 is located at a ~200 m lower elevation than the moraines of the ice-marginal position SW-14, the glacier in the main valley must have undergone a drastic thinning when it retreated from the ice-marginal position SW-14. ELA reconstructions cannot unambiguously answer whether the Katzensteig cirque glacier became disconnected from the main valley glacier at this time. As the equilibrium line of the Katzensteig glacier was situated at 1076 ± 18 m a.s.l. during formation moraines of the ice-marginal position KS-5, a lower ELA would have been required for joining the main valley glacier. If the moraine in the main valley formed at the margin of a combined glacier from the Wittenbach and Napf cirques, the ELA would have been 1106 ± 24 m a.s.l. Since we do not know whether the ELA was constant across the study area, it remains unclear whether the Katzensteig glacier still joined the glacier in the main valley. The CRE ages of the moraines of the ice-marginal positions SW-12 to -9 are indistinguishable from those of the SW-18, -17 and -15 moraines (range: 17.5 ± 1.0 to 16.0 ± 0.9 ka). ELA reconstructions reveal similar ELAs during the formation of these landforms. Small variations in the ELA were probably sufficient to trigger a progressive retreat of the glacier in the main valley.

If the sediment ridge at the entrance to the Wittenbach hanging valley is a terminal moraine, it is more likely that it formed at the margin of the Napf cirque glacier. Moraine formation at the margin of the Wittenbach cirque glacier would have required a lower ELA. As this view is not supported by the AAR-ELAs, ELA reconstructions do not allow for unambiguously attributing the moraine to one of the glaciers.

Both the CRE age of the SW-2 boulder and the reconstructed ELA suggest that the moraine of the ice-marginal positions SW-3 and -2 is related to a distinct glacial phase. First, the CRE age of the SW-2 boulder (14.0 ± 0.8 ka) does not overlap with that of the moraine of the ice-marginal position 9 (16.1 ± 0.7 ka). Second, the equilibrium line during moraine formation was situated at a significantly higher elevation (1195 ± 17 vs. 1126 ± 19 m a.s.l.).

Overlapping CRE ages suggest that the sampled moraines in the Katzensteig cirque probably formed at the same time (Figs. 4, 6 and 7). The ELA was probably 1150 m a.s.l. in the Katzensteig cirque, whereas it was probably higher (~1200 m a.s.l.) in the main valley (Figs. 6 and 7). Two factors could potentially explain the relatively low ELA in the Katzensteig cirque: the headwalls of the cirque are much steeper than the headwalls of the Wittenbach and Napf cirques. They are located east and NE of a hilly plateau extending from Hirschkopf (Fig. 1) in a westerly direction. Shading and snow drift from the west may have thus resulted in a locally lower

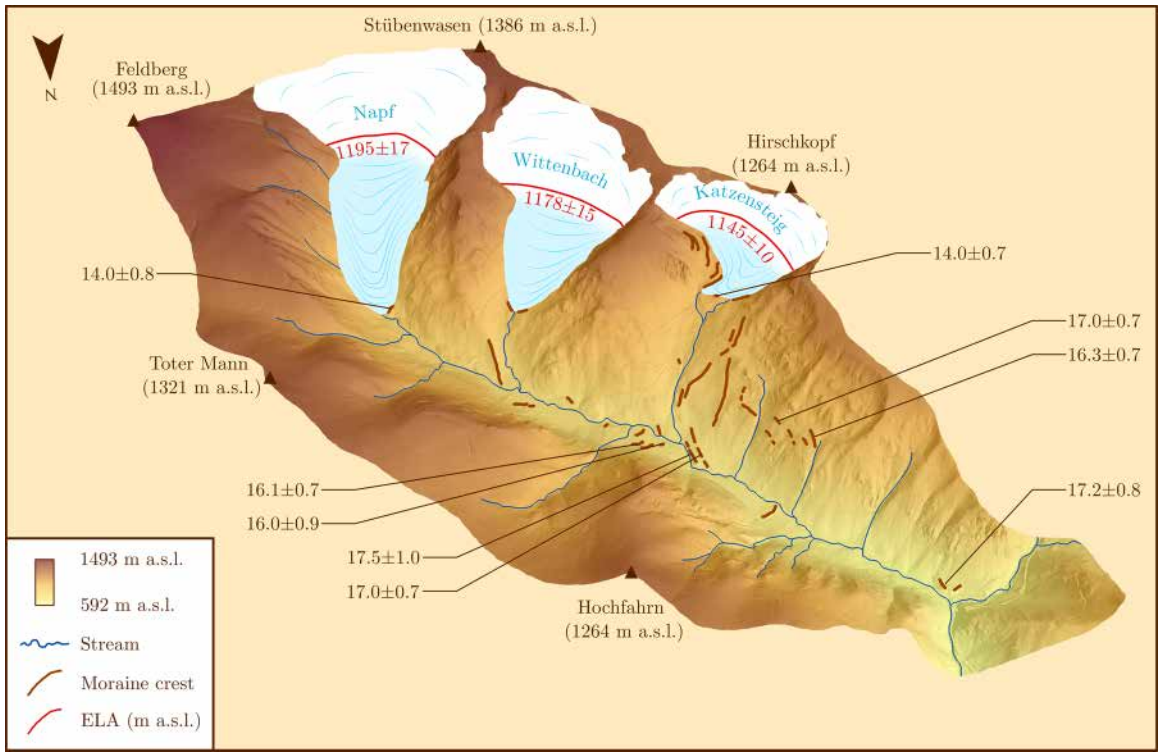

Figure 6. Moraines, glaciers and equilibrium line altitudes (ELAs) in the study area at around 14 ka. ^{10}Be CRE ages of moraines are presented in ka (thousand years before 2010 CE). [Color figure can be viewed at wileyonlinelibrary.com]

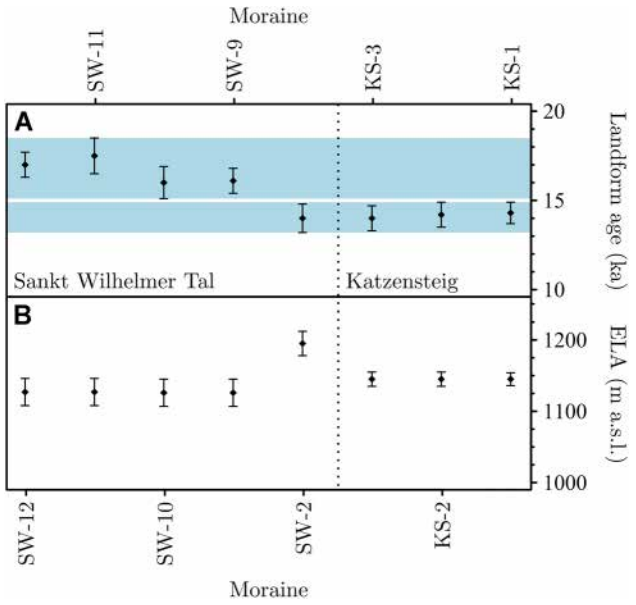

Figure 7. (A) ^{10}Be CRE ages of moraines and (B) ELAs during their formation. The landform ages indicate two phases of glacial re-advances and/or standstills during deglaciation of the study area (highlighted in light blue). [Color figure can be viewed at wileyonlinelibrary.com]

ELA. The ELA gradient across the study area precludes the idea that reconstructing ELAs of a few glaciers enables stratigraphical reconstructions. Determining a reliable relative age of the unsampled moraines in the Wittenbach hanging valley is therefore not possible. As demonstrated elsewhere (Tomkins *et al.*, 2018), Schmidt-Hammer exposure dating could be a suitable technique to resolve this issue. The equilibrium line then rose to a considerably higher elevation (1268 ± 13 m a.s.l.) and the moraine of the ice-marginal position SW-1 formed. Whether this moraine is related to a distinct glacial event remains unclear, as the lack of boulders prevents CRE dating of this landform.

Correlation with mountain glaciations in Central Europe

Here we compare the first deglaciation chronology from the Black Forest with existing chronologies from key localities in Central Europe (Fig. 8), which we base on 83 recalculated CRE ages from boulders on moraines (Fig. 9). Individual CRE ages are given in the Supporting Information (Table S2).

The timing of the maximum ice extent in the southern Black Forest during the Late Pleistocene remains unknown. Both CRE ages and ELA reconstructions imply two distinct phases of glacial re-advances and/or standstills during the subsequent deglaciation. During the first phase (not later than 17–16 ka), valley glaciers still existed in this region. They subsequently retreated further and disintegrated into small glaciers. The glaciation of the study area was restricted to the cirques by 14 ka at the latest.

Based on reasoning by analogy, Seret *et al.* (1990) proposed that the last glaciation maximum in the Vosges occurred at around 60 ka and, thus, considerably earlier than the last glacial maximum, irrespective of its definition (Hughes and Gibbard, 2015). Two moraines in the Wormsa Valley (Fig. 8) attributed to the last deglaciation gave CRE ages of 14.4 ± 1.6 and 13.6 ± 1.6 ka (Fig. 9B; Mercier *et al.*, 1999). As already mentioned by Kaltenbrunn and Preusser (2015), it is highly unlikely that a glacier persisted at an elevation of 525–550 m a.s.l. until ~14 ka and, hence, the ages probably reflect post-depositional processes. An erratic boulder on a moraine in the Altenbach Valley further north (Fig. 8) yielded a CRE age of 22.5 ± 1.9 ka (Fig. 9C; Mercier *et al.*, 1999). Moraines in the Missheimle cirque, one of four cirques in the upper reaches of the valley, stabilized at the latest at 19.3 ± 1.5 and at 16.8 ± 1.5 ka (Fig. 9C; Mercier *et al.*, 1999). A later glacial

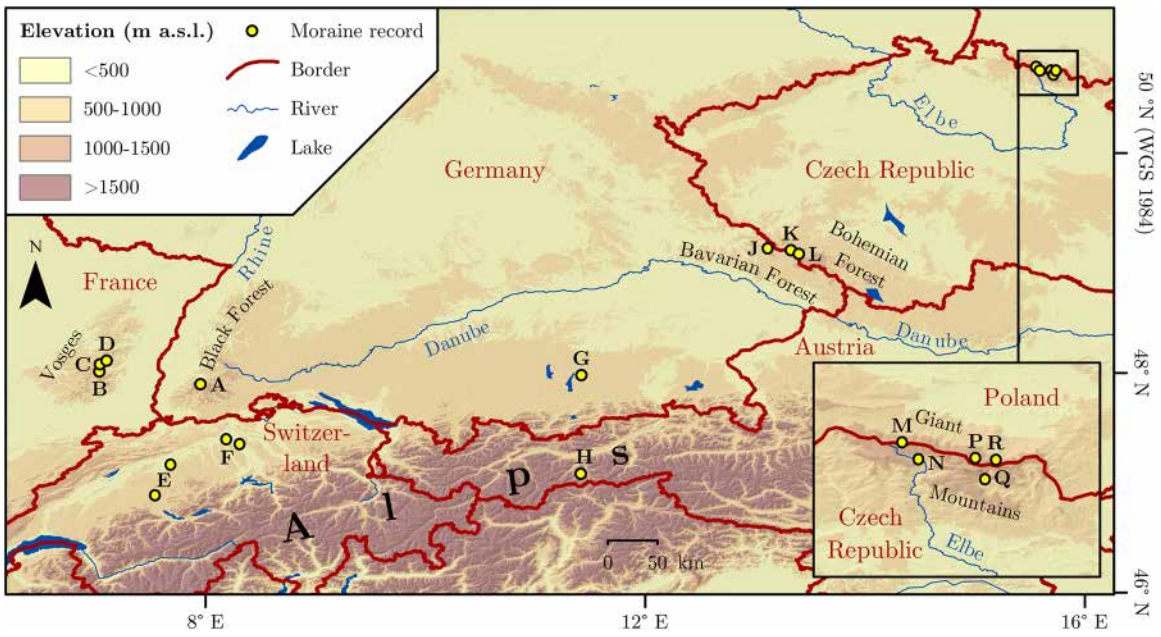

Figure 8. Key sites in the mountain regions of Central Europe and their forelands where terminal moraines were sampled for ^{10}Be CRE dating: (A) Sankt Wilhelmer Tal (this study); (B) Wormsa Valley (Vosges); (C) Altenbach Valley and Missheimle cirque (Vosges); (D) Lac Noir cirque; (E) Aare Valley; (F) Lenzburg and Wohlen; (G) Lake Starnberg; (H) Gschnitz Valley (European Alps); (J) Kleiner Arbersee (Bavarian Forest); (K) Laka Valley (Bohemian Forest); (L) Prášilské Valley (Bohemian Forest); (M) Snowy cirques (Giant Mountains); (N) Labský důl (Giant Mountains); (P) Łomnica Valley (Giant Mountains); (Q) Úpa Valley (Giant Mountains); (R) Łomniczka Valley (Giant Mountains). See Fig. 9 for references. The CRE ages were recalculated for this study and are presented in Fig. 9 and in the Supporting Information. The shaded relief in the background was derived from elevation data acquired during the SRTM (Jarvis *et al.*, 2008). © EuroGeographics for the administrative boundaries. [Color figure can be viewed at wileyonlinelibrary.com]

re-advance or standstill in the Lac Noir cirque further north (Fig. 8) occurred no later than 14.7 ± 1.5 ka (Fig. 9D; Mercier *et al.*, 1999).

Last glaciation maximum moraines in the northern foreland of the Alps (in the Aare valley and at Lenzburg; Fig. 8) formed not later than 22.9 ± 1.4 and 21.5 ± 1.0 ka, respectively (Fig. 9E,F; Ivy-Ochs *et al.*, 2004; Reber *et al.*, 2014). The CRE ages are thus slightly younger than radiocarbon and optically stimulated luminescence ages from the same region, suggesting a last glaciation maximum at around 25 ka (Gaar *et al.*, 2019, and references therein). The CRE ages are also younger than radiocarbon ages from the southern foreland of the Alps, pointing to a Late Pleistocene maximum glacier extent at around 26–24 ka (Monegato *et al.*, 2007, 2017). Although CRE ages from the area around Lake Starnberg further east (Fig. 8) seemingly suggest a later Late Pleistocene glaciation maximum (Fig. 9G), these ages (18.1 ± 1.2 and 17.7 ± 1.0 ka) are not consistent with independent chronological evidence. Post-depositional processes, such as boulder tilting, probably explain the underestimated CRE ages (Reuther *et al.*, 2011).

CRE ages from moraines inside the Late Pleistocene maximum ice extent in the northern foreland of the Alps (near Wohlen and in the Aare valley around the city of Bern; Fig. 8) document glacial re-advances and/or standstills not later than 19.5 ± 1.3, 18.2 ± 1.0 and 17.4 ± 0.8 ka (Fig. 9E,F; Reber *et al.*, 2014; Wüthrich *et al.*, 2018). The first unequivocal glacial re-advance in the Alps took place during the Gschnitz stadial when roughly 80–90% of the ice volume in the Alps had already been disappeared (Ivy-Ochs *et al.*, 2008). According to CRE ages from the stratotype in the Gschnitz Valley (Fig. 8), this stadial occurred at the latest at 17.9 ± 1.0 ka (Fig. 9H; Ivy-Ochs *et al.*, 2006).

The furthest Late Pleistocene glacier advance in the area around Kleiner Arbersee (Bavarian Forest) culminated at the latest at 21.0 ± 1.0 ka (Fig. 9J; Reuther, 2007). Subsequent glacial re-advances and/or standstills occurred not later than 20.3 ± 1.0, 18.8 ± 0.8 and 16.9 ± 1.1 ka (Fig. 9J; Reuther, 2007). An unsampled moraine further upvalley from the lake could be related to a younger glacial phase. Moraines at similar elevations also occur at other localities in the Bavarian Forest, but they have hitherto not been sampled for ^{10}Be CRE dating (Hauner *et al.*, 2019).

On the Czech side of the mountains (Bohemian Forest), there is more robust evidence for later glacier oscillations. CRE ages from the Laka Valley (Fig. 8) suggest moraine formation at the latest at 15.8 ± 1.8 and 13.8 ± 1.3 ka (Fig. 9K; Mentlík *et al.*, 2013). Concomitant glacier fluctuations also occurred in the Prášilské Valley several kilometres further SE (Fig. 8) where moraines stabilized not later than 15.4 ± 0.7 and 13.4 ± 1.2 ka (Fig. 9L; Mentlík *et al.*, 2013). The CRE ages of the innermost moraine are confirmed by a basal radiocarbon age in a sediment core from a nearby lake (Stará Jímka) pointing to ice-free conditions at around 14 ka (Mentlík *et al.*, 2010). The Late Pleistocene glaciation maximum in this area occurred at the latest at 17.5 ± 1.4 ka (Fig. 9L; Mentlík *et al.*, 2013).

Multiple sets of CRE ages from the Giant Mountains have been published. The Late Pleistocene maximum glacier advance in the area downvalley from the snowy cirques (Śnieżne Kotły; Fig. 8) occurred not later than 18.4 ± 1.0 ka (Fig. 9M; Engel *et al.*, 2014). The next further upvalley moraine formed by 18.1 ± 0.9 ka at the latest. Note that Schmidt Hammer rebound values from these moraines and those further upvalley as well as the moraines' morphology suggest that these CRE ages are probably underestimated (Engel *et al.*, 2014). Further periods of moraine formation occurred not later than 18.4 ± 0.7, 13.6 ± 1.2, 12.0 ± 0.5 and 11.5 ± 0.7 ka (Fig. 9M). The snowy cirques are thus the only localities where CRE ages document moraine formation after the climatic downturn in Central Europe at around 12.9 ka evidenced elsewhere (see Heiri *et al.*, 2014, and references therein). The Late Pleistocene maximum glacier advance in the uppermost Elbe Valley (Labský důl) further SE culminated not later than 17.5 ± 1.5 ka (Fig. 9N; Mercier *et al.*, 2000). This

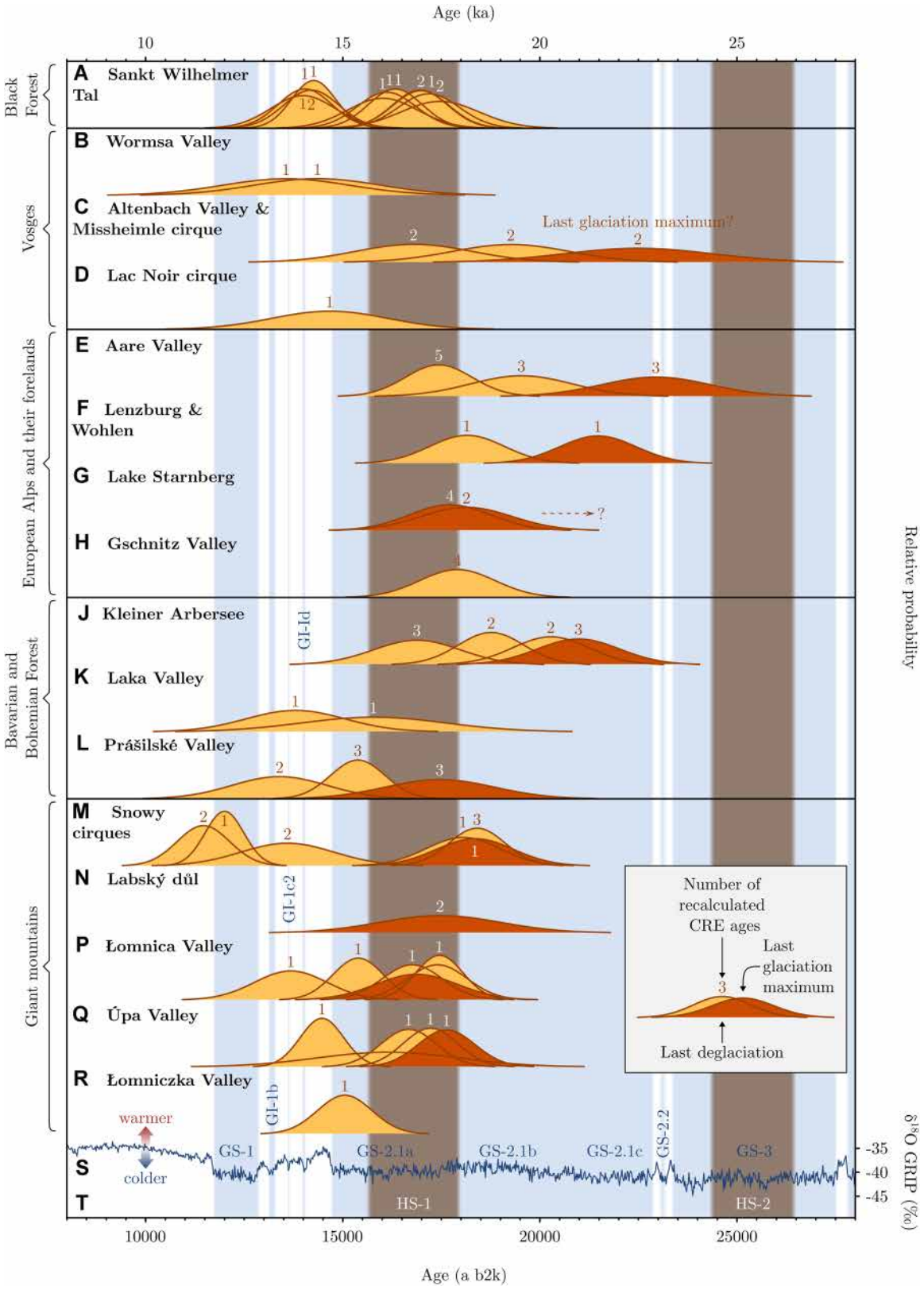

Figure 9. Probability density functions of periods of moraine formation in (A) Sankt Wilhelmer Tal (this study), (B) the Wormsa Valley (Vosges; Mercier *et al.*, 1999), (C) the Altenbach Valley and one cirque in its upper part, the Missheimle cirque (Vosges; Mercier *et al.*, 1999), (D) the Lac Noir cirque (Vosges; Mercier *et al.*, 1999), (E) the Aare Valley (northern foreland of the European Alps; Ivy-Ochs *et al.*, 2004; Wüthrich *et al.*, 2018), at (F) Lenzburg and Wohlen (northern foreland of the Alps; Reber *et al.*, 2014), (G) in the area around Lake Starnberg (northern forelands of the Alps; Reuther, 2007), (H) the Gschnitz Valley (Eastern Alps; Ivy-Ochs *et al.*, 2006), (J) at Kleiner Arbersee (Bavarian Forest; Reuther, 2007), (K) in the Laka Valley (Bohemian Forest; Mentlík *et al.*, 2013), (L) in the Prášilské Valley (Bohemian Forest; Mentlík *et al.*, 2013), (M) in the snowy cirques (Giant Mountains; Engel *et al.*, 2014), (N) in Labský důl (Giant Mountains; Mercier *et al.*, 2000), (P) in the Łomnica Valley (Giant Mountains; Engel *et al.*, 2011), (Q) in the Úpa Valley (Giant Mountains; Engel *et al.*, 2014) and (R) in the Łomniczka Valley (Giant Mountains; Engel *et al.*, 2011) according to recalculated ^{10}Be CRE ages. See Fig. 8 for a map of the sites. The CRE ages were not corrected for denudation, vegetation cover or snow shielding. As mentioned in the text, the CRE ages of the moraines at Lake Starnberg are probably distant minimum ages of the landforms. (S) Greenland stadials (GS) and interstadials (GI) according to the INTIMATE event stratigraphy (Rasmussen *et al.*, 2014) as well as δ^{18}O (20-year mean) with respect to Vienna Standard Mean Ocean Water (V-SMOW) in the Greenland Ice Core Project (GRIP) ice core (Johnsen *et al.*, 1997; Rasmussen *et al.*, 2014; Seierstad *et al.*, 2014) are shown for comparison. (T) Heinrich Stadials (HS) according to Sanchez Goñi and Harrison (2010): HS-2 (26.5–24.3 ka) and HS-1 (18.0–15.6 ka). [Color figure can be viewed at wileyonlinelibrary.com]

minimum age broadly agrees with CRE ages of two last glaciation maximum moraines in the Łomnica Valley further east (Fig. 8) that stabilized by 16.9 ± 1.0 and 16.8 ± 0.8 ka at the latest (Fig. 9P; Engel *et al.*, 2011). Moraines further upvalley formed not later than 17.5 ± 0.6, 17.4 ± 0.8, 15.4 ± 0.6 and 13.7 ± 0.9 ka (Fig. 9P; Engel *et al.*, 2011). The oldest CRE ages from moraines in the Úpa Valley further SE suggest periods of moraine formation not later than 17.6 ± 0.7, 17.2 ± 0.7, 16.1 ± 1.8 and 14.5 ± 0.6 ka (Fig. 9Q; Engel *et al.*, 2014). CRE dating of a terminal moraine in the Łomniczka Valley on the Polish side of the mountains (Fig. 8) resulted in a CRE age of 15.1 ± 0.7 ka (Fig. 9R; Engel *et al.*, 2011).

Within the limits of available data, the variation of the ^{10}Be CRE ages from last glaciation maximum moraines tentatively indicates that the Late Pleistocene glaciation maxima in the mountains of Central Europe and their forelands could have been asynchronous. Figure 9 reveals that the last glaciation maximum in the Giant Mountains no later than 18–17 ka (Mercier *et al.*, 2000; Engel *et al.*, 2011, 2014) may have occurred later than the Late Pleistocene glaciation maximum in the foreland of the Alps (22.9 ± 1.4 and 21.5 ± 1.0 ka; Ivy-Ochs *et al.*, 2004; Reber *et al.*, 2014). Unfortunately, this study could not clarify whether the Late Pleistocene glaciation maximum in the Black Forest was synchronous with a last glaciation maximum evidenced elsewhere. Testing the hypothesis of asynchronous last glaciation maxima urgently requires CRE ages from moraines of this phase in the southern Black Forest and in other mountainous regions of Central Europe.

As shown in Fig. 9, CRE ages from moraines of the first phase of glacier advances and/or standstills during the deglaciation of the study area overlap with those of moraines in the Missheimle cirque (16.8 ± 1.5 ka), in the Aare Valley (Bern stade; 17.4 ± 0.8 ka), in the Gschnitz Valley (17.9 ± 1.0 ka), at Kleiner Arbersee (16.9 ± 1.1 ka), in the Łomnica Valley (17.4 ± 0.8 and 17.5 ± 0.6 ka) and in the Úpa Valley (16.1 ± 1.8 ka). Those from moraines of the second phase of glacier activity during the deglaciation of the study area are indistinguishable from CRE ages from moraines in the Lac Noir cirque (14.7 ± 1.5 ka), the Laka Valley (13.8 ± 1.3 ka), the Prášilské Valley (13.4 ± 1.2 ka), the snowy cirques (13.6 ± 1.2 ka), the Łomnica Valley (13.7 ± 0.9 ka) and in the Úpa Valley (14.5 ± 0.6 ka).

The presence of moraines of a similar age at different sites suggest that the periods of moraine formation might be related to climatic phases that affected at least major parts of Central Europe. Ivy-Ochs *et al.* (2006) already proposed that the Gschnitz stadial should be regarded as the response to Heinrich Event 1, a phase of massive iceberg discharge into the North Atlantic (Heinrich, 1988; Bond *et al.*, 1992; Clark *et al.*, 2012) between 18.0 and 15.6 ka (Fig. 9T; Sanchez Goñi and Harrison, 2010). Relatively low δ^{18}O values in the Greenland Ice Core Project ice core indicate that cool conditions prevailed at this time (Fig. 9S; Johnsen *et al.*, 1997). Reuther *et al.* (2011) speculated that the formation of the innermost sampled moraine at Kleiner Arbersee is potentially related to this cool period in the North Atlantic region. The second phase of glacial re-advances and/or standstills during the deglaciation of the study area could be linked to cool phases before the climatic amelioration in Central Europe starting at around 14.6 ka (Heiri *et al.*, 2014, and references therein).

However, these hypotheses remain tentative for now. Before glacial phases can be robustly correlated with climatic events, we propose that three main issues need to be resolved: first, a more extensive set of CRE ages from the southern Black Forest must be acquired to evaluate whether the glacial phases described here are of regional relevance. This will also allow the establishment of a regional stratigraphy of the last glaciation according to the guidelines of Hughes *et al.* (2005). Second, existing data from other mountainous regions, particularly chronological data from other records and ELAs, need to be reviewed in more detail for a more holistic view of interdependencies. Third, future work will have to clarify whether moraines formed during climatically controlled glacial advances or during standstills triggered by factors other than climate, such as the retreat to more shaded areas (e.g. Lukas, 2007).

Conclusions

Geomorphological mapping, CRE dating and ELA reconstructions allowed for reconstructing the Late Pleistocene glacial history of the southern Black Forest in unprecedented detail. Geomorphological mapping revealed 18 ice-marginal positions in the main valley and multiple ice-marginal positions in the tributary valleys. For the first time, ^{10}Be CRE dating was applied to moraines in the Black Forest and revealed that two discrete phases of glacial re-advances and/or standstills occurred during the deglaciation of the study area. The moraine of the outermost securely identified ice-marginal position formed not later than 17 ka. Overlapping CRE ages indicate further periods of moraine formation no later than 17–16 ka. The ELA was situated at 1110–1140 m a.s.l. during these glacial events. Moraines in the cirques formed during the second phase of glacier activity by 14 ka at the latest when the ELA was situated between 1150 and 1200 m a.s.l. The ELA gradient in the study area suggests strongly that ELAs should not be used for local stratigraphical correlations. Future studies will have to clarify whether the periods of moraine formation proposed here are also documented at other sites in the Black Forest. Furthermore, techniques for determining relative ages of moraines, such as Schmidt Hammer exposure dating, should be tested.

The newly acquired CRE ages significantly enhance the knowledge of glaciation in the mountain regions of Central Europe. Periods of moraine formation in the study area are also documented at other sites in Central Europe. These phases may have been triggered by cooling in the North Atlantic region, but a further assessment requires disentangling climatically driven glacier variations and those caused by other factors such as topographic effects. In addition, there is an urgent need for additional chronological data and for dating the last glaciation maximum in the southern Black Forest, as this phase is apparently not preserved in the study area.

Supporting information

Additional supporting information can be found in the online version of this article. This article includes online-only Supplemental Data.

Appendix S1. Detailed sample documentation.

Table S1. Input-sheet for the online CREp calculator.

Table S2. Recalculated ^{10}Be CRE ages from terminal moraines at key sites in mountainous regions in Central Europe and their forelands.

Acknowledgements. F.M.H. is in receipt of a PhD scholarship of *Studienstiftung des Deutschen Volkes*. This study was also financially supported by the German Research Foundation through the 'Geometry, chronology and dynamics of the last Pleistocene glaciation of the Black Forest' project (PR 957/3-1) granted to F.P. Florian Rauscher and Alexander Fülling are acknowledged for their support during fieldwork. The farmers and landowners, particularly Martin Rudiger, Roland Klingele and Philipp Hansul, are thanked for their permission for sampling. The forestry department of the Breisgau-Hochschwarzwald district provided a forest access permit. The nature protection department as well as the forest policy and conservation department of *Regierungspräsidium Freiburg* are acknowledged for the permission to obtain samples for ^{10}Be CRE dating in the Feldberg natural reserve

and in the Faulbach *Bannwald*. Régis Braucher is thanked for providing unpublished data for the review of CRE ages from moraines in Central Europe. This paper benefited from insightful discussions with Stefan Hergarten on ELA reconstructions. The French AMS national facility ASTER (CEREGE, Aix-en-Provence) is supported by the INSU/CNRS, the ANR through the 'Projets thématiques d'excellence' programme for the 'Equipements d'excellence' ASTER-CEREGE action and IRD. This paper is dedicated to the late Didier Bourlès, who greatly supported this study. Unfortunately, he was not able to discuss the results with us. The reviewers are thanked for their thoughtful comments that greatly helped to improve the quality of the manuscript. The authors declare that they have no conflicts of interest. Open access funding enabled and organized by Projekt DEAL.

Data Availability Statement

The detailed sample documentation, the methodology of the review of previously published ^{10}Be CRE ages, the input-sheet for the CREp online calculator as well as the recalculated ^{10}Be CRE ages are provided in the Supporting Information. All other data are available from the corresponding author upon reasonable request.

Abbreviations. ASTER, Accélérateur pour les Sciences de la Terre, Environnement, Risques; AABR, area–altitude balance ratio; AAR, accumulation area ratio; AMS, accelerator mass spectrometry; CEREGE, Centre Européen de Recherche et d'Enseignement des Geosciences de l'Environnement; CRE, cosmic ray exposure; DEM, digital elevation model; DTM, digital terrain model; ELA, equilibrium line altitude; GS, Greenland stadial; HS, Heinrich stadial; LGM, Last Glacial Maximum; LN_2C, Laboratoire National des Nucléides Cosmogéniques; SRTM, Shuttle Radar Topography Mission; V-SMOW, Vienna Standard Mean Ocean Water.

References

Ahnert F. 2009. *Einführung in die Geomorphology*. Ulmer.

Andreoli R, Rosique T, Schmidt M *et al*. 2006. La dernière phase glaciaire du haut bassin de la Fecht (Vosges, France): dynamique de l'englacement et chronologie relative de la déglaciation. *Géomorphologie: Relief, Processus, Environnement* **12**: 23–36. https://doi.org/10.4000/geomorphologie.455

Arnold M, Aumaître G, Bourlès DL *et al*. 2013. The French accelerator mass spectrometry facility ASTER after 4 years: status and recent developments on ^{36}Cl and ^{129}I. *Nuclear Instruments and Methods in Physics Research Section B* **294**: 24–28. https://doi.org/10.1016/j.nimb.2012.01.049

Arnold M, Merchel S, Bourlès DL *et al*. 2010. The French accelerator mass spectrometry facility ASTER: improved performance and developments. *Nuclear Instruments and Methods in Physics Research Section B* **268**: 1954–1959. https://doi.org/10.1016/j.nimb.2010.02.107

Bakke J, Nesje A. 2011. Equilibrium-line altitude (ELA). In *Encyclopedia of Snow, Ice and Glaciers*, Singh VP, Singh P, Haritashya UK (eds). Springer Netherlands: Dordrecht; 268–277.

Balco G. 2007. CRONUS-Earth Al-26/Be-10 exposure age calculator MATLAB function reference Version 2: November 2007. http://hess.ess.washington.edu/math/docs/al_be_v2/al_be_fctn_desc [accessed 15 July 2021].

Balco G. 2011. Contributions and unrealized potential contributions of cosmogenic-nuclide exposure dating to glacier chronology, 1990–2010. *Quaternary Science Reviews* **30**: 3–27. https://doi.org/10.1016/j.quascirev.2010.11.003

Balco G. 2017. *Documentation – v3 exposure age calculator*. https://sites.google.com/a/bgc.org/v3docs. [accessed 15 July 2021].

Balco G. 2018. *Topographic shielding calculator*. stoneage.ice-d.org/math/skyline/skyline_in.html. [accessed 27 August 2020].

Balco G, Stone JO, Lifton NA *et al*. 2008. A complete and easily accessible means of calculating surface exposure ages or erosion rates from ^{10}Be and ^{26}Al measurements. *Quaternary Geochronology* **3**: 174–195. https://doi.org/10.1016/j.quageo.2007.12.001

Barr ID, Lovell H. 2014. A review of topographic controls on moraine distribution. *Geomorphology* **226**: 44–64. https://doi.org/10.1016/j.geomorph.2014.07.030

Becker A, Ammann B, Anselmetti FS *et al*. 2006. Paleoenvironmental studies on Lake Bergsee, Black Forest, Germany. *Neues Jahrbuch für Geologie und Paläontologie – Abhandlungen* **240**: 405–445. https://doi.org/10.1127/njgpa/240/2006/405

Benn DI, Hulton NRJ. 2010. An ExcelTM spreadsheet program for reconstructing the surface profile of former mountain glaciers and ice caps. *Computers and Geosciences* **36**: 605–610. https://doi.org/10.1016/j.cageo.2009.09.016

Bond G, Heinrich H, Broecker W *et al*. 1992. Evidence for massive discharges of icebergs into the North Atlantic Ocean during the last glacial period. *Nature* **360**: 245–249. https://doi.org/10.1038/360245a0

Boston CM, Lukas S, Carr SJ. 2015. A Younger Dryas plateau icefield in the Monadhliath, Scotland, and implications for regional palaeoclimate. *Quaternary Science Reviews* **108**: 139–162. https://doi.org/10.1016/j.quascirev.2014.11.020

Boulton GS, Morris EM, Armstrong AA *et al*. 1979. Direct measurement of stress at the base of a glacier. *Journal of Glaciology* **22**: 3–24. https://doi.org/10.3189/S0022143000014027

Braucher R, Guillou V, Bourlès DL *et al*. 2015. Preparation of ASTER in-house ^{10}Be/^{9}Be standard solutions. *Nuclear Instruments and Methods in Physics Research Section B* **361**: 335–340. https://doi.org/10.1016/j.nimb.2015.06.012

Bronk Ramsey C. 2009. Bayesian analysis of radiocarbon dates. *Radiocarbon* **51**: 337–360. https://doi.org/10.1017/S0033822200033865

Chmeleff J, von Blanckenburg F, Kossert K *et al*. 2010. Determination of the ^{10}Be half-life by multicollector ICP-MS and liquid scintillation counting. *Nuclear Instruments and Methods in Physics Research Section B* **268**: 192–199. https://doi.org/10.1016/j.nimb.2009.09.012

Clark PU, Shakun JD, Baker PA *et al*. 2012. Global climate evolution during the last deglaciation. *Proceedings of the National Academy of Sciences of the United States of America* **109**: E1134–E1142. https://doi.org/10.1073/pnas.1116619109 [PubMed: 22331892]

Claude A, Ivy-Ochs S, Kober F *et al*. 2014. The Chironico landslide (Valle Leventina, southern Swiss Alps): age and evolution. *Swiss Journal of Geosciences* **107**: 273–291. https://doi.org/10.1007/s00015-014-0170-z

Cohen D, Hooke RL, Iverson NR *et al*. 2000. Sliding of ice past an obstacle at Engabreen, Norway. *Journal of Glaciology* **46**: 599–610. https://doi.org/10.3189/172756500781832747

Duphorn K. 1968. Ist der Oberharz im Pleistozän vergletschert gewesen? *E&G Quaternary Science Journal* **19**: 164–174. https://doi.org/10.3285/eg.19.1.10

Duprat-Oualid F, Rius D, Bégeot C *et al*. 2017. Vegetation response to abrupt climate changes in Western Europe from 45 to 14.7k cal a BP: the Bergsee lacustrine record (Black Forest, Germany). *Journal of Quaternary Science* **32**: 1008–1021. https://doi.org/10.1002/jqs.2972

Engel Z, Braucher R, Traczyk A *et al*. 2014. ^{10}Be exposure age chronology of the last glaciation in the Krkonoše Mountains, Central Europe. *Geomorphology* **206**: 107–121. https://doi.org/10.1016/j.geomorph.2013.10.003

Engel Z, Traczyk A, Braucher R *et al*. 2011. Use of ^{10}Be exposure ages and Schmidt hammer data for correlation of moraines in the Krkonoše Mountains, Poland/Czech Republic. *Zeitschrift für Geomorphologie* **55**: 175–196. https://doi.org/10.1127/0372-8854/2011/0055-0036

Erb L. 1948. Die Geologie des Feldbergs. In *Der Feldberg im Schwarzwald*, Müller K (ed). L. Bielefelds Verlag KG: Freiburg; 22–96.

Ergenzinger P. 1967. Die eiszeitliche Vergletscherung des Bayerischen Waldes. *E&G Quaternary Science Journal* **18**: 152–168. https://doi.org/10.3285/eg.18.1.10

Friedmann A. 1998/9. Pollenanalytische Untersuchungen zur holozänen Vegetations- und Landschaftsgeschichte des westlichen Hochschwarzwalds. *Berichte der Naturforschenden Gesellschaft zu Freiburg i. Br.* 88/89: 57–84.

Gaar D, Graf HR, Preusser F. 2019. New chronological constraints on the timing of Late Pleistocene glacier advances in northern Switzerland. *E&G Quaternary Science Journal* **68**: 53–73. https://doi.org/10.5194/egqsj-68-53-2019

Glaser R, Schönbein J, Wang Q. 2013. Die 'gemäßigten Breiten' – Europa klimatisch. In *Europa – eine Geographie*, Gebhardt H, Glaser R, Lentz S (eds). Springer Spektrum: Berlin; 50–65.

Gosse JC, Phillips FM. 2001. Terrestrial in situ cosmogenic nuclides: theory and application. *Quaternary Science Reviews* **20**: 1475–1560. https://doi.org/10.1016/S0277-3791(00)00171-2

Gross G, Kerschner H, Patzelt G. 1977. Methodische Untersuchungen über die Schneegrenze in alpinen Gletschergebieten. *Zeitschrift für Gletscherkunde und Glazialgeologie* **12**: 223–251.

Haase E. 1966. Eine Erinnerung an Karl Schimper. *Berichte der Naturforschenden Gesellschaft zu Freiburg i. Br.* **56**(2), 151–154.

Hann HP, Schreiner A, Zedler H. 2011. *Geologische Karte von Baden-Württemberg 1: 25 000. Blatt 8113 Todtnau. 1: 25,000. Landesamt für Geologie, Rohstoffe und Bergbau: Freiburg im Breisgau.*

Hauner U, Lehrberger G, Brugger M. 2019. *Der Naturraum Bayerischer Wald – Šumava in Den Eiszeiten*. Nationalparkverwaltung Bayerischer Wald: Grafenau.

Heinrich H. 1988. Origin and consequences of cyclic ice rafting in the northeast Atlantic Ocean during the past 130,000 years. *Quaternary Research* **29**: 142–152. https://doi.org/10.1016/0033-5894(88)90057-9

Heiri O, Koinig KA, Spötl C *et al.* 2014. Palaeoclimate records 60–8 ka in the Austrian and Swiss Alps and their forelands. *Quaternary Science Reviews* **106**: 186–205. https://doi.org/10.1016/j.quascirev.2014.05.021

Hemmerle H, May J-H, Preusser F. 2016. Übersicht über die pleistozänen Vergletscherungen des Schwarzwaldes. *Berichte der Naturforschenden Gesellschaft zu Freiburg i. Br.* **106**: 31–67.

Heyman J, Applegate PJ, Blomdin R *et al.* 2016. Boulder height – exposure age relationships from a global glacial ^{10}Be compilation. *Quaternary Geochronology* **34**: 1–11. https://doi.org/10.1016/j.quageo.2016.03.002

Hilger P, Gosse JC, Hermanns RL. 2019. How significant is inheritance when dating rockslide boulders with terrestrial cosmogenic nuclide dating? – a case study of an historic event. *Landslides* **16**: 729–738. https://doi.org/10.1007/s10346-018-01132-0

Hofmann FM, Alexanderson H, Schoeneich P *et al.* 2019. Post-Last Glacial Maximum glacier fluctuations in the southern Écrins massif (westernmost Alps): insights from ^{10}Be cosmic ray exposure dating. *Boreas* **48**: 1019–1041. https://doi.org/10.1111/bor.12405

Hofmann FM, Rauscher F, McCreary W *et al.* 2020. Revisiting Late Pleistocene glacier dynamics north-west of the Feldberg, southern Black Forest, Germany. *E&G Quaternary Science Journal* **69**(1), 61–87. https://doi.org/10.5194/egqsj-69-61-2020

Hughes PD, Gibbard PL. 2015. A stratigraphical basis for the Last Glacial Maximum (LGM). *Quaternary International* **383**: 174–185. https://doi.org/10.1016/j.quaint.2014.06.006

Hughes PD, Gibbard PL, Woodward JC. 2005. Quaternary glacial records in mountain regions: A formal stratigraphical approach. *Episodes* **28**: 85–92. https://doi.org/10.18814/epiiugs/2005/v28i2/002

Hüttner R. 1967. Das Quartär. In *Geologische Karte von Baden-Württemberg 1:25 000, Erläuterungen zu Blatt 8013 Freiburg-Südost*, Geologisches Landesamt Baden-Württemberg (ed). Landesvermessungsamt Baden-Württemberg: Stuttgart; 69–105.

Ivy-Ochs S, Kerschner H, Kubik PW *et al.* 2006. Glacier response in the European Alps to Heinrich Event 1 cooling: the Gschnitz stadial. *Journal of Quaternary Science* **21**: 115–130. https://doi.org/10.1002/jqs.955

Ivy-Ochs S, Kerschner H, Reuther A *et al.* 2008. Chronology of the last glacial cycle in the European Alps. *Journal of Quaternary Science* **23**: 559–573. https://doi.org/10.1002/jqs.1202

Ivy-Ochs S, Kober F. 2008. Surface exposure dating with cosmogenic nuclides. *E&G Quaternary Science Journal* **57**: 179–209. https://doi.org/10.3285/eg.57.1-2.7

Ivy-Ochs S, Schäfer J, Kubik PW *et al.* 2004. Timing of deglaciation on the northern Alpine foreland (Switzerland). *Eclogae Geologicae Helvetiae* **97**: 47–55. https://doi.org/10.1007/s00015-004-1110-0

Jarvis A, Reuter HI, Nelson A *et al.* 2008 *Hole-Filled SRTM for the Globe* version 4. srtm.csi.cgiar.org. [accessed 30 June 2021].

Johnsen SJ, Clausen HB, Dansgaard W *et al.* 1997. The δ^{18}O record along the Greenland Ice Core Project deep ice core and the problem of possible Eemian climatic instability. *Journal of Geophysical Research: Oceans* **102**: 26397–26410. https://doi.org/10.1029/97JC00167

Kaltenbrunn A, Preusser F. 2015. Überblick über die quartären Vergletscherungen der Vogesen. *Berichte der Naturforschenden Gesellschaft zu Freiburg i. Br.* **105**: 9–35.

Kern Z, László P. 2010. Size specific steady-state accumulation-area ratio: an improvement for equilibrium-line estimation of small palaeoglaciers. *Quaternary Science Reviews* **29**: 2781–2787. https://doi.org/10.1016/j.quascirev.2010.06.033

Kerschner H, Ivy-Ochs S. 2008. Palaeoclimate from glaciers: examples from the Eastern Alps during the Alpine Lateglacial and Early Holocene. *Global and Planetary Change* **60**: 58–71. https://doi.org/10.1016/j.gloplacha.2006.07.034

Korschinek G, Bergmaier A, Faestermann T *et al.* 2010. A new value for the half-life of ^{10}Be by Heavy-Ion Elastic Recoil Detection and liquid scintillation counting. *Nuclear Instruments and Methods in Physics Research Section B* **268**: 187–191. https://doi.org/10.1016/j.nimb.2009.09.020

Krause D, Margold M. 2019. Glacial geomorphology of the Šumava/Bayerischer Wald mountains, Central Europe. *Journal of Maps* **15**(2), 719–725. https://doi.org/10.1080/17445647.2019.1661881

Kubik PW, Ivy-Ochs S, Masarik J *et al.* 1998. ^{10}Be and ^{26}Al production rates deduced from an instantaneous event within the dendrocalibration curve, the landslide of Köfels, Ötz Valley, Austria. *Earth and Planetary Science Letters* **161**: 231–241. https://doi.org/10.1016/S0012-821X(98)00153-8

Lal D. 1991. Cosmic ray labeling of erosion surfaces: in situ nuclide production rates and erosion models. *Earth and Planetary Science Letters* **104**: 424–439. https://doi.org/10.1016/0012-821X(91)90220-C

Lang G. 2005. *Seen und Moore des Schwarzwaldes als Zeugen spätglazialen und holozänen Vegetationswandels. Stratigraphische, pollenanalytische und großrestanalytische Untersuchungen*. Staatliches Museum für Naturkunde Karlsruhe: Karlsruhe.

Lang G, Merkt J, Streif H 1984. Spätglazialer Gletscherrückzug und See- und Moorentwicklung im Südschwarzwald, Südwestdeutschland. *Dissertationes Botanicae* **72** (Festschrift Max Welten): 213–234.

Le Roy M, Deline P, Carcaillet J *et al.* 2017. ^{10}Be exposure dating of the timing of Neoglacial glacier advances in the Ecrins-Pelvoux massif, southern French Alps. *Quaternary Science Reviews* **178**: 118–138. https://doi.org/10.1016/j.quascirev.2017.10.010

Li Y-K. 2018. Determining topographic shielding from digital elevation models for cosmogenic nuclide analysis: a GIS model for discrete sample sites. *Journal of Mountain Science* **15**: 939–947. https://doi.org/10.1007/s11629-018-4895-4

Liehl E. 1982. Landschaftsgeschichte des Feldberggebietes. In Der Feldberg im Schwarzwald: Subalpine Insel im Mittelgebirge, Landesanstalt für Umweltschutz Baden-Württemberg, Institut für Ökologie und Naturschutz (ed.). Karlsruhe; 13-147.

Lukas S. 2007. Early-Holocene glacier fluctuations in Krundalen, south central Norway: palaeoglacier dynamics and palaeoclimate. *Holocene* **17**: 585–598. https://doi.org/10.1177/0959683607078983

Mackintosh AN, Anderson BM, Pierrehumbert RT. 2017. Reconstructing climate from glaciers. *Annual Review of Earth and Planetary Sciences* **45**: 649–680. https://doi.org/10.1146/annurev-earth-063016-020643

Maier A, Stojakowits P, Mayr C *et al.* 2021. Cultural evolution and environmental change in Central Europe between 40 and 15 ka. *Quaternary International* **581–582**: 225–240. https://doi.org/10.1016/j.quaint.2020.09.049

Martin LCP, Blard P-H, Balco G *et al.* 2017. The CREp program and the ICE-D production rate calibration database: a fully parameterizable and updated online tool to compute cosmic-ray exposure ages. *Quaternary Geochronology* **38**: 25–49. https://doi.org/10.1016/j.quageo.2016.11.006

Masarik J, Wieler R. 2003. Production rates of cosmogenic nuclides in boulders. *Earth and Planetary Science Letters* **216**: 201–208. https://doi.org/10.1016/S0012-821X(03)00476-X

Mentlík P, Engel Z, Braucher R *et al.* 2013. Chronology of the Late Weichselian glaciation in the Bohemian Forest in Central Europe. *Quaternary Science Reviews* **65**: 120–128. https://doi.org/10.1016/j.quascirev.2013.01.020

Mentlík P, Minár J, Břízová E *et al.* 2010. Glaciation in the surroundings of Prášilské Lake (Bohemian Forest, Czech Republic). *Geomorphology* **117**: 181–194. https://doi.org/10.1016/j.geomorph.2009.12.001

Mercier J-L, Bourlès DL, Kalvoda J *et al.* 1999. Deglaciation of the Vosges dated using ^{10}Be. *Acta Universitatis Carolinae, Geographica* **2**: 139–155.

Mercier J-L, Jeser N. 2004. The glacial history of the Vosges Mountains. In *Quaternary Glaciations Extent and Chronology - Part I: Europe*, Ehlers J, Gibbard PL (eds). Elsevier: Amsterdam; 113–118.

Mercier J-L, Kalvoda J, Bourlès DL *et al*. 2000. Preliminary results of ^{10}Be dating of glacial landscape in the Giant Mountains. *Acta Universitatis Carolinae Geographica, Supplementum* **35**: 157–170.

Metz B, Saurer H. 2012. Geomorphology und Landschaftsentwicklung. In *Der Feldberg: Subalpine Insel im Schwarzwald*, Regierungspräsidium Freiburg (ed.). Jan Thorbecke Verlag der Schwabenverlag AG: Ostfildern; 14–62.

Monegato G, Ravazzi C, Donegana M *et al*. 2007. Evidence of a two-fold glacial advance during the Last Glacial Maximum in the Tagliamento end moraine system (Eastern Alps). *Quaternary Research* **68**: 284–302. https://doi.org/10.1016/j.yqres.2007.07.002

Monegato G, Scardia G, Hajdas I *et al*. 2017. The Alpine LGM in the boreal ice-sheets game. *Scientific Reports* **7**: 2078. https://doi.org/10.1038/s41598-017-02148-7 [PubMed: 28522806]

Muscheler R, Beer J, Kubik PW *et al*. 2005. Geomagnetic field intensity during the last 60,000 years based on ^{10}Be and ^{36}Cl from the Summit ice cores and ^{14}C. *Quaternary Science Reviews* **24**: 1849–1860. https://doi.org/10.1016/j.quascirev.2005.01.012

NASA Jet Propulsion Laboratory. 2013. *NASA Shuttle Radar Topography Mission Global 1 arc second*. https://doi.org/10.5067/MEaSUREs/SRTM/SRTMGL1.003 [accessed 31 May 2021].

Nishiizumi K, Winterer EL, Kohl CP *et al*. 1989. Cosmic ray production rates of ^{10}Be and ^{26}Al in quartz from glacially polished rocks. *Journal of Geophysical Research* **94**: 17907–17915. https://doi.org/10.1029/JB094iB12p17907

Paterson WSB. 1970. The sliding velocity of Athabasca Glacier, Canada. *Journal of Glaciology* **9**: 55–63. https://doi.org/10.3189/S0022143000026794

Paterson WSB. 1994. *The Physics of Glaciers*. Pergamon Press: Oxford.

Pearce DM, Ely JC, Barr ID *et al*. 2017. Glacier reconstruction. In *Geomorphological Techniques*, Clarke LE, Nield JM (eds). British Society for Geomorphology: London.

Pellitero R, Rea BR, Spagnolo M *et al*. 2015. A GIS tool for automatic calculation of glacier equilibrium-line altitudes. *Computers and Geosciences* **82**: 55–62. https://doi.org/10.1016/j.cageo.2015.05.005

Pellitero R, Rea BR, Spagnolo M *et al*. 2016. GlaRe, a GIS tool to reconstruct the 3D surface of palaeoglaciers. *Computers and Geosciences* **94**: 77–85. https://doi.org/10.1016/j.cageo.2016.06.008

Rasmussen SO, Bigler M, Blockley SP *et al*. 2014. A stratigraphic framework for abrupt climatic changes during the Last Glacial period based on three synchronized Greenland ice-core records: refining and extending the INTIMATE event stratigraphy. *Quaternary Science Reviews* **106**: 14–28. https://doi.org/10.1016/j.quascirev.2014.09.007

Rea BR. 2009. Defining modern day area-altitude balance ratios (AABRs) and their use in glacier-climate reconstructions. *Quaternary Science Reviews* **28**: 237–248. https://doi.org/10.1016/j.quascirev.2008.10.011

Rea BR, Pellitero R, Spagnolo M *et al*. 2020. Atmospheric circulation over Europe during the Younger Dryas. *Science Advances* **6**(50), https://doi.org/10.1126/sciadv.aba4844 [PubMed: 33310841]

Reber R, Akçar N, Ivy-Ochs S *et al*. 2014. Timing of retreat of the Reuss Glacier (Switzerland) at the end of the Last Glacial Maximum. *Swiss Journal of Geosciences* **107**: 293–307. https://doi.org/10.1007/s00015-014-0169-5

Reimer PJ, Austin WEN, Bard E *et al*. 2020. The IntCal20 Northern Hemisphere Radiocarbon Age Calibration Curve (0–55 cal kBP). *Radiocarbon* **62**: 725–757. https://doi.org/10.1017/RDC.2020.41

Reinig F, Wacker L, Jöris O *et al*. 2021. Precise date for the Laacher See eruption synchronizes the Younger Dryas. *Nature* **595**: 66–69. https://doi.org/10.1038/s41586-021-03608-x [PubMed: 34194020]

Reitner JM, Ivy-Ochs S, Drescher-Schneider R *et al*. 2016. Reconsidering the current stratigraphy of the Alpine Lateglacial: implications of the sedimentary and morphological record of the Lienz area (Tyrol/Austria). *E&G Quaternary Science Journal* **65**(2), 113–144. https://doi.org/10.3285/eg.65.2.02

Reuther AU. 2007. *Surface exposure dating of glacial deposits from the last glacial cycle. Evidence from the Eastern Alps, the Bavarian Forest, the Southern Carpathians and the Altai Mountains*. Borntraeger: Berlin.

Reuther AU, Fiebig M, Ivy-Ochs S *et al*. 2011. Deglaciation of a large piedmont lobe glacier in comparison with a small mountain glacier – new insight from surface exposure dating. Two studies from SE Germany. *E&G Quaternary Science Journal* **60**: 248–269. https://doi.org/10.3285/eg.60.2-3.03

Sanchez Goñi MF, Harrison SP. 2010. Millennial-scale climate variability and vegetation changes during the Last Glacial: concepts and terminology. *Quaternary Science Reviews* **29**: 2823–2827. https://doi.org/10.1016/j.quascirev.2009.11.014

Sawatzki G. 1992. *Geologische Karte 1: 25 000 von Baden-Württemberg. Erläuterungen zu Blatt 8214 St. Blasien*. Landesvermessungsamt Baden-Württemberg: Stuttgart.

Schreiner A. 2011. Quartär. In *Geologische Karte von Baden-Württemberg 1:25 000. Erläuterungen zu Blatt 8113 Todtnau*, Landesamt für Geologie, Rohstoffe und Bergbau (LGRB) (ed). Landesamt für Geologie, Rohstoffe und Bergbau (LGRB): Freiburg i. Br; 42–92.

Seierstad IK, Abbott PM, Bigler M *et al*. 2014. Consistently dated records from the Greenland GRIP, GISP2 and NGRIP ice cores for the past 104 ka reveal regional millennial-scale δ18O gradients with possible Heinrich event imprint. *Quaternary Science Reviews* **106**: 29–46. https://doi.org/10.1016/j.quascirev.2014.10.032

Seret G, Dricot E, Wansard G. 1990. Evidence for an early glacial maximum in the French Vosges during the last glacial cycle. *Nature* **346**: 453–456. https://doi.org/10.1038/346453a0

Sissons JB. 1974. A late-glacial ice cap in the central Grampians, Scotland. *Transactions of the Institute of British Geographers* **62**: 95–114. https://doi.org/10.2307/621517

Steinmann G. 1902. Die Bildungen der Letzten Eiszeit im Bereiche des alten Wutachgebiets. *Berichte des oberrheinischen Geologischen Vereins* **35**: 1–8.

Stokes CR, Tarasov L, Blomdin R *et al*. 2015. On the reconstruction of palaeo-ice sheets: recent advances and future challenges. *Quaternary Science Reviews* **125**: 15–49. https://doi.org/10.1016/j.quascirev.2015.07.016

Stone JO. 2000. Air pressure and cosmogenic isotope production. *Journal of Geophysical Research: Solid Earth* **105**: 23753–23759. https://doi.org/10.1029/2000JB900181

Tomkins MD, Dortch JM, Hughes PD *et al*. 2018. Rapid age assessment of glacial landforms in the Pyrenees using Schmidt hammer exposure dating (SHED). *Quaternary Research* **90**: 26–37. https://doi.org/10.1017/qua.2018.12

Tomkins MD, Dortch JM, Hughes PD *et al*. 2021. Moraine crest or slope: an analysis of the effects of boulder position on cosmogenic exposure age. *Earth and Planetary Science Letters* **570**. https://doi.org/10.1016/j.epsl.2021.117092 [PubMed: 117092]

Uppala SM, Kållberg PW, Simmons AJ *et al*. 2005. The ERA-40 reanalysis. *Quarterly Journal of the Royal Meteorological Society* **131**: 2961–3012. https://doi.org/10.1256/qj.04.176

Vočadlová K, Petr L, Žáčková P *et al*. 2015. The Lateglacial and Holocene in Central Europe: a multi-proxy environmental record from the Bohemian Forest, Czech Republic. *Boreas* **44**: 769–784. https://doi.org/10.1111/bor.12126

Woillard GM. 1978. Grande pile peat bog: A continuous pollen record for the last 140,000 years. *Quaternary Research* **9**: 1–21. https://doi.org/10.1016/0033-5894(78)90079-0

Wüthrich L, Morabito EG, Zech J *et al*. 2018. ^{10}Be surface exposure dating of the last deglaciation in the Aare Valley, Switzerland. *Swiss Journal of Geosciences* **111**: 295–303. https://doi.org/10.1007/s00015-018-0298-3

Zweck C, Zreda M, Desilets D. 2013. Snow shielding factors for cosmogenic nuclide dating inferred from Monte Carlo neutron transport simulations. *Earth and Planetary Science Letters* **379**: 64–71. https://doi.org/10.1016/j.epsl.2013.07.023

